



**UNIVERSIDAD DE INVESTIGACIÓN DE TECNOLOGÍA
EXPERIMENTAL YACHAY**

Escuela de Ciencias Físicas y Nanotecnología

**TÍTULO: BIOSENSOR BASED ON TiO₂-MWCNTS FOR
HYDROGEN PEROXIDE DETECTION**

Trabajo de integración curricular presentado como requisito para la
obtención del título de Ingeniero en Nanotecnología

Autor:

Guerrero León L. Andrés

Tutor:

Ph.D. González Vásquez Gema

Urququí, agosto de 2019

Urcuquí, 20 de agosto de 2019

SECRETARÍA GENERAL
(Vicerrectorado Académico/Cancillería)
ESCUELA DE CIENCIAS FÍSICAS Y NANOTECNOLOGÍA
CARRERA DE NANOTECNOLOGÍA
ACTA CONSOLIDADA DE FINALIZACIÓN DE ESTUDIOS No. UITEY-PHY-2019-00007-AC

En la ciudad de San Miguel de Urcuquí, Provincia de Imbabura, a los 20 días del mes de agosto de 2019, se emite la presente acta consolidada de finalización de estudios, conforme lo establecido en el artículo 101 del Reglamento de Régimen Académico aprobado por el Consejo de Educación Superior (CES), mediante resolución RPC-SO-08-No.111-2019, de 27 de febrero de 2019.

DATOS DE IDENTIFICACIÓN DEL ESTUDIANTE

Documento de Identificación	Apellidos y Nombres	Carrera
1104671159	GUERRERO LEON, LENIN ANDRES	NANOTECNOLOGÍA

SUFICIENCIA DE LA LENGUA EXTRANJERA

Conforme lo establecido en el artículo 31 del Reglamento de Régimen Académico aprobado por el Consejo de Educación Superior (CES), mediante resolución RPC-SE-13-No.051-2013, de 22 de marzo de 2017: (...) las IES garantizarán el nivel de suficiencia del idioma para cumplir con el requisito de graduación de las carreras de nivel técnico superior, tecnológico superior y sus equivalentes; y, tercer nivel, de grado, deberán organizar u homologar las asignaturas correspondientes desde el inicio de la carrera. La suficiencia de la lengua extranjera deberá ser evaluada antes de que el estudiante se matricule en el último periodo académico ordinario de la respectiva carrera; tal prueba será habilitante para la continuación de sus estudios, sin perjuicio de que este requisito pueda ser cumplido con anterioridad. (...) En las carreras de tercer nivel, de grado, se entenderá por suficiencia en el manejo de una lengua extranjera al menos el nivel correspondiente a B2 del Marco Común Europeo de referencia para las Lenguas. (...)

Calificación	Nivel Alcanzado
80	B2



Mgs. MONTAÑO ORMAZA, DENNYS EDUARDO
Director del Departamento de Inglés

PRÁCTICAS PRE-PROFESIONALES O PASANTÍAS

Conforme lo establecido en los artículos 82, 89, 94 del Reglamento de Régimen Académico aprobado por el Consejo de Educación Superior (CES), mediante resolución RPC-SE-13-No.051-2013, de 22 de marzo de 2017.

Vinculación

Empresa	Nombre Proyecto	Horas	Fecha Inicio	Fecha Fin
UNIDAD EDUCATIVA VICTOR MANUEL GUZMAN	INSPIRATHON	160	08/10/2018	08/12/2018
Total Horas Cumplidas:		160		

Prácticas

Empresa	Horas	Fecha Inicio	Fecha Fin
UNIVERSIDAD DE INVESTIGACIÓN DE TECNOLOGÍA EXPERIMENTAL YACHAY	240	01/10/2017	31/12/2017
Total Horas Cumplidas:		240	



Dra. SALUM, GRACIELA MARISA, Ph.D.
Presidenta de la Comisión de Prácticas Pre-Profesionales y Vinculación con la Sociedad

REGISTRO DE CALIFICACIONES

Conforme lo establecido en el artículo 24 del Reglamento de Titulación de Grado de la Universidad de Investigación de Tecnología Experimental Yachay, en el que establece: La calificación final de grado del estudiante se obtendrá calculando de la siguiente manera: 1. El 70% corresponderá al promedio ponderado de calificaciones obtenidas por el estudiante a lo largo de toda su carrera y que se calculará en relación con el número de horas totales asignadas a cada asignatura en la correspondiente malla curricular distribuido así: a) El 20% para las asignaturas del "Tronco Común"; y, b) El 50% para las asignaturas propias de cada Carrera incluyendo los itinerarios. 2. El 30% restante corresponderá a la calificación de la defensa del trabajo de titulación o del examen teórico – práctico.

Fecha de Inicio: 28/10/2014 Fecha de Finalización: 20/08/2019

	Promedio	Horas	Créditos	Porcentaje	Calificación
Tronco Común	7,8			20 %	1,6
Carrera	8,8	8368	215	50 %	4,4
Defensa	10			30 %	3
Calificación Final de Grado:				100 %	9


Mgs. CASANOVA YANDUN, EDISON GUILLERMO
Director de Registros Académicos

RECONOCIMIENTO ACADÉMICO

Conforme lo establecido en el artículo 34 del Reglamento de Titulación de Grado de la Universidad de Investigación de Tecnología Experimental Yachay, aprobado mediante Resolución No.RCG-SE-10 No.036-2018 de 28 de septiembre de 2018: "(...) Las ceremonias de graduación colectiva serán organizadas por las autoridades de la Universidad de Investigación de Tecnología Experimental Yachay, en las que se otorgará las siguientes distinciones: Summa cum laude (Promedios entre 9.7 y 10), Magna cum laude (Promedios entre 9.4 y 9.6) y Cum laude (Promedios entre 9 a 9.3)". Ante lo cual, se otorga el reconocimiento académico " CUM LAUDE ", por haber obtenido la calificación de 9 Sobre 10.

TITULACIÓN

Una vez se ha verificado el cumplimiento de los requisitos establecidos en el artículo 31 del Reglamento de Titulación de Grado de la Universidad de Investigación de Tecnología Experimental Yachay, aprobado mediante Resolución No.RCG-SE-10 No.036-2018 de 28 de septiembre de 2018, se confiere el título de INGENIERO/A EN NANOTECNOLOGÍA, a el(la) señor(ita) GUERRERO LEON, LENIN ANDRES.

Desde la fecha de suscripción de la presenta acta, conforme lo establecido en el artículo 101 del Reglamento de Régimen Académico aprobado por el Consejo de Educación Superior (CES), mediante resolución RPC-SO-08-No.111-2019, de 27 de febrero de 2019; la Universidad de Investigación de Tecnología Experimental Yachay, tiene un plazo de cuarenta y cinco (45) días para registrar el título en el Sistema Nacional de Información de la Educación Superior (SNIESE), previa entrega al graduado.

Para constancia de lo actuado, firman el Secretario General, el Decano de la Escuela y el/la Estudiante.


Dr. BRITO GONZALVEZ, JOAQUIN LUIS, Ph.D.
Secretario General

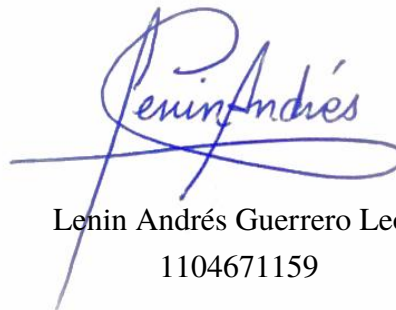

Dr. MEDINA DAGGER, ERNESTO ANTONIO, Ph.D.
Decano


GUERRERO LEON, LENIN ANDRES
Estudiante

Autoría

Yo, LENIN ANDRÉS GUERRERO LEÓN, con cédula de identidad 1104671159, declaro que las ideas, juicios, valoraciones, interpretaciones, consultas bibliográficas, definiciones y conceptualizaciones expuestas en el presente trabajo; así como, los procedimientos y herramientas utilizadas en la investigación, son de absoluta responsabilidad de el/la autora (a) del trabajo de integración curricular. Así mismo, me acojo a los reglamentos internos de la Universidad de Investigación de Tecnología Experimental Yachay.

Urcuquí, agosto de 2019




Lenin Andrés Guerrero León
1104671159

Autorización de Publicación

Yo, LENIN ANDRÉS GUERRERO LEÓN, con cédula de identidad 1104671159, cedo a la Universidad de Tecnología Experimental Yachay, los derechos de publicación de la presente obra, sin que deba haber un reconocimiento económico por este concepto. Declaro además que el texto del presente trabajo de titulación no podrá ser cedido a ninguna empresa editorial para su publicación u otros fines, sin contar previamente con la autorización escrita de la Universidad.

Asimismo, autorizo a la Universidad que realice la digitalización y publicación de este trabajo de integración curricular en el repositorio virtual, de conformidad a lo dispuesto en el Art. 144 de la Ley Orgánica de Educación Superior.

Urcuquí, agosto de 2019



Lenin Andrés Guerrero León
1104671159

Acknowledgements

This research was funded by CEDIA (Corporación Ecuatoriana para el Desarrollo de la Investigación y la Academia) through the project "Biosensores basados en Nanotubos de carbono modificados para detección de enzimas", Code: CEPRA XII-2018-14, Biosensores.

I would like to thank my supervisor, Ph.D. Gema González Vásquez, for her invaluable cooperation in the formulation and development of my thesis and further dissertation at Yachay Tech, always willing to help me. Also, I would like to thank my co-advisor, Ph.D. Mayra Peralta Arcia for her continuous corrections and concern to improve everytime my work.

A very special gratitude to Pontificia Universidad Católica del Ecuador, specifically to my tutors Ph.D. Patricio Espinoza and Ph.D. Lenys Fernandez for helping and providing the facilities and supplies to develop my work, in addition to their assistance and support.

Also, I would like to thank to Instituto Venezolano de Investigaciones Científicas, Universidad Simón Bolívar and Escuela Politécnica Nacional for providing their facilities to complete a crucial section of my work.

Finally, I would like thank to my family for always holding my back along the university; and to my lab partner D. Jeréz, who was a support in deliberating over our problems and findings. And, last but not least: Bones, Lorelayf and MJ.

To everyone else, remember: with great power, comes great responsibility. And thank you.

Andrés Guerrero

Resumen

El objetivo de la siguiente tesis de investigación es diseñar y evaluar un biosensor de peróxido de hidrógeno H_2O_2 basado en nanotubos de carbono de pared múltiple dopados con nanoestructuras de dióxido de titanio (TiO_2 -MWCNT). La construcción del electrodo fue realizada sobre una superficie de carbón vítreo modificada con TiO_2 -MWCNT, Azul de Prusia como electrocatalizador y PDDA como estabilizador electrostático. Nanotubos de carbono funcionalizados (fMWCNT) y TiO_2 -MWCNTs fueron caracterizados usando TEM, FTIR y XRD confirmando la presencia de anatasa sobre los nanotubos de carbono. La técnica Potencial Zeta fue empleada para determinar la carga superficial en las dos muestras de nanotubos. Dependiendo de la carga superficial, el solvente, que optimiza la dispersión de los nanotubos, fue seleccionado: dimetil formamida (DMF) para los fMWCNTs y dodecilsulfato sódico para TiO_2 -MWCNTs. El electrodo modificado fue además caracterizado usando voltametría cíclica y amperometría. Estas técnicas demostraron la reducción típica de H_2O_2 electrocatalizada a través del Azul de Prusia. Los fMWCNTs exhibieron una sensibilidad (s) de $16.30 \mu A/mM$ y un límite de detección (LOD) de $0.015 mM L^{-1}$, respecto a los TiO_2 -MWCNTs, donde se obtuvieron valores de $s=26.51 \mu A/mM$ y $LOD= 0.092 mM L^{-1}$.

Palabras Clave: biosensor electroquímico, peróxido de hidrógeno, nanotubos de carbono, nanoestructuras de titania, voltametría cíclica.

Abstract

The aim of this thesis is the designing and evaluation of a hydrogen peroxide (H_2O_2) biosensor based on modified multi-walled carbon nanotubes with titanium dioxide nanostructures (TiO_2 -MWCNT). The construction of the electrode was performed over a glassy carbon surface, modified with TiO_2 -MWCNT, Prussian Blue as electro-catalyzer, and poly(diallyldimethylammonium chloride) (PDDA) as electrostatic stabilizer. Functionalized MWCNTs (fMWCNTs) and TiO_2 -MWCNTs were characterized using TEM, FTIR and XRD confirming the presence of anatase over the carbon nanotubes. Zeta potential was used to determine the surface charge on both CNTs samples. Depending on the surface charge, a solvent, which optimizes the CNTs dispersion, was selected: dimethyl formamide (DMF) for fMWCNTs and sodium dodecylsulfate (SDS) for TiO_2 -MWCNTs. The modified electrode was also characterized through electrochemical techniques: cyclic voltammetry and amperometry. These techniques demonstrated the typical reduction of the H_2O_2 electrocatalyzed through Prussian Blue. The fMWCNTs exhibited a sensitivity of $s=16.30 \mu\text{A}/\text{mM}$ and a limit of detection of $\text{LOD}= 0.015 \text{ mM L}^{-1}$ respect to TiO_2 -MWCNTs with values of $s=26.51 \mu\text{A}/\text{mM}$ and $\text{LOD}= 0.092 \text{ mM L}^{-1}$.

Keywords: electrochemical biosensor, hydrogen peroxide, titania doped carbon nanotubes, cyclic voltammetry

Contents

List of Figures	xix
List of Tables	xxi
1 Introduction	1
1.1 Problem Statement	2
1.2 General and Specific Objectives	3
2 Theoretical Background	5
2.1 What are Nanomaterials?	5
2.1.1 Carbon Nanotubes	6
2.1.2 Titanium Dioxide	7
2.2 Biosensors	7
2.2.1 Nanomaterials in Biosensors	8
2.3 Prussian Blue and its Catalytic Activity	9
2.4 Quantitative Measurement	10
2.5 Electrochemical Techniques	10
2.5.1 Cyclic Voltammetry	11
2.5.2 Chronoamperometry	11
2.5.3 Zeta Potential	12
2.5.4 Amperometry (i-t Curve)	13
2.6 Literature Review	15

2.6.1	Carbon Nanotubes-based Biosensors	15
2.6.2	TiO ₂ & TiO ₂ /Carbon Nanotubes-based Biosensor	16
3	Methodology	19
3.1	Electrochemical Equipment	19
3.1.1	Reagents and Solutions	19
3.1.2	Electrochemical Cell and Electrodes	20
3.1.3	Hardware and Software	21
3.2	Nanostructures Synthesis	21
3.2.1	Functionalization of Carbon Nanotubes	21
3.2.2	Synthesis of TiO ₂ -CNT Nanostructures	22
3.3	Characterization of Carbon Nanotubes	22
3.3.1	Transmission Electron Microscopy	22
3.3.2	Fourier Transform Infrared Spectroscopy	22
3.3.3	X-Ray Diffraction	22
3.3.4	Zeta Potential	23
3.4	Electrode Modification	23
3.4.1	Electrode Polishing	23
3.4.2	Dispersion of Carbon Nanotubes	24
3.4.3	Modification of PDDA/CNT/GC Electrode	24
3.4.4	Modification of PDDA/TiO ₂ -CNT/GC Electrode	24
3.4.5	Electrodeposition and Activation of Prussian Blue	25
3.4.6	Peroxide Detection	25
3.5	Electrochemical Characterization	27
3.5.1	TiO ₂ -CNTs and fCNTs/GCE Characterization	27
3.5.2	Prussian Blue-modified GCE Characterization	29
4	Results & Discussion	31
4.1	Physical Characterization of TiO ₂ -CNT and fCNT Nanostructures	32
4.2	Zeta Potential and Carbon Nanotubes Dispersion	36
4.3	Direct electrochemistry of modified and non-modified electrodes	39
4.4	Evaluation response of modified and non-modified electrode in a redox system	41

4.5	Electrochemistry of PB/CNT/GCE and PB/fCNT/GCE in presence of hydrogen peroxide via cyclic voltammetry	46
4.6	Evaluation response of PB/TiO ₂ -CNT/GCE and PB/fCNT/GCE in presence of hydrogen peroxide via amperometric i-t curve	51
5	Conclusions	55
	Bibliography	57

List of Figures

2.1	Diagrams of a single-walled carbon nanotube and a multi-walled carbon nanotube. ¹	6
2.2	Scheme of components of a biosensor.	8
2.3	Prussian Blue molecule	9
2.4	Applied potential as a function of time to perform a cycling sweep.	12
2.5	Chronoamperometry excitation waveform of voltage along time	13
2.6	Scheme of the electrochemical double layer at the solid-liquid interface	14
3.1	Scheme of PDDA/PB/PDDA/TiO ₂ -CNTs/GC electrode modification.	26
4.1	TEM images of functionalized carbon nanotubes	33
4.2	TEM images of TiO ₂ -CNT at different magnifications	33
4.3	XRD diffractograms of (a) TiO ₂ -CNT and (b) fCNTs.	34
4.4	FTIR spectra of TiO ₂ -CNTs and fCNTs.	35
4.5	Zeta potential result for fCNTs.	37
4.6	Zeta potential result for TiO ₂ -CNTs.	38
4.7	Electroactive region of glassy carbon electrode, fCNTs-GCE and TiO ₂ -CNTs-GCE on PBS pH 7.	40
4.8	Cyclic voltammeteries of the different GCE modifications at a scan rate of 100 mV/s.	42
4.9	Set of cyclic voltammeteries of the bGCE at different scan rates and linear regression of anodic and cathodic peak currents	43
4.10	Set of cyclic voltammeteries of fCNT at different scan rates and linear regression of anodic and cathodic peak currents	44
4.11	Set of cyclic voltammeteries of TiO ₂ -CNT at different scan rates and linear regression of anodic and cathodic peak currents	45

4.12	Set of cyclic voltammetries of PB-CNT at different scan rates and linear regression of anodic and cathodic peak currents	45
4.13	Set of cyclic voltammetries of PB-TiO ₂ -CNT at different scan rates and linear regression of anodic and cathodic peak currents	46
4.14	Set of cyclic voltammetries of PB-fCNT at different H ₂ O ₂ concentrations. Reduction of anodic peak of Prussian Blue as H ₂ O ₂ concentration increases. Increment of cathodic peak of Prussian Blue as H ₂ O ₂ concentration increases.	47
4.15	Set of cyclic voltammetries of PB-fCNT at different H ₂ O ₂ concentrations at a reduced potential range. Reduction of anodic peak of Prussian Blue as H ₂ O ₂ concentration increases. Increment of cathodic peak of Prussian Blue as H ₂ O ₂ concentration increases.	48
4.16	Set of cyclic voltammetries of fCNT at different H ₂ O ₂ concentrations.	49
4.17	Set of cyclic voltammetries of PB-TiO ₂ -CNT at different H ₂ O ₂ concentrations.	50
4.18	Dynamic response of the H ₂ O ₂ on fCNT/GC electrode to the successive addition H ₂ O ₂ at 0.5 V. Calibration curve of the amperometric response between the current and H ₂ O ₂ concentration.	52
4.19	Dynamic response of the H ₂ O ₂ on TiO ₂ -CNT/GC electrode to the successive addition H ₂ O ₂ at 0.5 V. Calibration curve of the amperometric response between the current and H ₂ O ₂ concentration.	53

List of Tables

3.1	Quantities of reactives to prepare different H ₂ O ₂ concentrated solutions	26
3.2	Parameters to detect H ₂ O ₂ via CV in PBS	28
3.3	Parameters to measure the amperometric response of the sensor to hydrogen peroxide in 20 mL of PBS	28
3.4	Parameters of cyclic voltammetry over the bare and modified GCE in 25 mL of PBS pH 7	29
3.5	Parameters of cyclic voltammetry over bare and modified electrodes in a 4 mM potassium ferricyanide solution.	30
3.6	Parameters in CV to analyze the reaction kinetics of Prussian Blue-modified electrodes in PBS.	30
4.1	Summary of the electrodes, layers and designations employed in the work	32

Chapter 1

Introduction

The use of nanomaterials in biosensing have become a subject of intense research, having a significant impact in everyday life². Carbon nanotubes (CNTs) are at the forefront of this intense research reflecting unique and remarkable mechanical, thermal, electrical and elastic properties^{3,4}. These properties include for example, flexible characteristics that can contrast from being a semiconductor to a conductor⁵. Recent studies demonstrated that carbon nanotubes enhance the electrochemical reactivity of important biomolecules and improve the electron transfer; these properties make them suitable for a wide range of applications including the development of biosensors⁶. Nanomaterials are used in biosensors to enhance the bioanalytical performance or offer innovative routes of interfacing the transduction processes in the development of electrochemical biosensor⁷, a device which is able to provide quantitative measurements, using a biological recognition element which is in contact with an electrochemical transduction component⁸.

Nanostructured metal oxides have been found to exhibit strong adsorption ability, catalytic properties and biocompatibility, making them ideal for biosensor development and offering excellent interfaces for biological recognition⁹. Metal oxides nanoparticles attached onto the carbon nanotubes surface are also receiving notable interest because the potential applications designing electrochemically functional nanostructures³, which include higher surface area and better biocompatibility; and help addressing the design of a biosensing interface allowing the analyte to interact effectively over the biosensing surface.

Titanium dioxide (TiO_2) has shown tremendous interests in promising areas such as photovoltaics, biosensing and photocatalysis¹⁰. TiO_2 nanostructures exhibit large surface area, and unique chemical and electronic properties¹¹. From the stoichiometry theory for semiconductors, TiO_2 is electron rich, belonging to n-type semiconductor kind. TiO_2 nanomaterials have been used for sensors in detection of soluble organics in aqueous media; besides gas, chemicals and biological substances detection¹¹.

Hydrogen peroxide (H_2O_2) is one of the most common analytes because of its importance in biological, environmental and industrial processes. In the human body, H_2O_2 is able to be converted in hydroxyl radical ($-\text{OH}$), which is highly reactive¹². The overproduction of these reactive species such as hydroxyl ion and superoxide O_2^- in the cellular interstices is demonstrated to promote cell damage and tissue malfunction¹³. Also, hydrogen peroxide detection forms the diagnosis response of medical devices such glucose sensors because in presence of oxygen, H_2O_2 is produced by the action of glucose oxidase^{14,15}. Hydrogen peroxide is also found in foodstuff and drinking water as well as its use in waste treatment and bleaching applications¹⁶.

1.1 Problem Statement

The presence of hydrogen peroxide in everyday life such as glucose monitors, foodstuff, bleaching processes, even in the regulation of human processes, plays an important role among the detection of analytes. Therefore, the design of a biosensor should accomplish some parameters as versatility, high sensitivity and fast response.

One of the challenges in biosensing is to successfully design an interface between the analyte and the electrode surface⁷. In the matter of enzyme-based biosensors, the immobilization of the enzyme denotes an enormous task to lead the communication between its active site and the analyte. Furthermore the remarkable properties mentioned above, the presence of modified carbon nanotubes could lead to an improved route of interfacing and a superior response in H_2O_2 detection.

The evaluation of TiO_2 -MWCNT modified electrodes, and Prussian Blue as artificial perox-

idase will help to design a model of electrode to analyze the performance and contribution of carbon nanotubes and titanium dioxide nanostructures in the detection of hydrogen peroxide.

1.2 General and Specific Objectives

Focused on the main characteristics that a biosensor should accomplish, such as versatility, high sensitivity, high selectivity, faster signal and rapid detection; the general objective of this work is:

The design and evaluation of a hydrogen peroxide biosensor based on carbon nanotubes modified with titanium dioxide nanostructures.

In the development of the peroxide biosensor, the specific objectives to accomplish the valid construction of the biosensor are:

- Characterize functionalized and modified carbon nanotubes using physical methods: SEM, FTIR, XRD and Z-Potential.
- Design an interface based in layers to couple the functionalized and modified carbon nanotubes over a glassy carbon electrode.
- Characterize the bare and modified glassy carbon electrode via cyclic voltammetry.
- Evaluate Prussian Blue mechanism modified electrodes through hydrogen peroxide detection via cyclic voltammetry and amperometric curves.
- Analyze the redox behavior of the Prussian blue layer in the modified glassy carbon electrode.
- Analyze the redox behavior and hydrogen peroxide detection through calculation of sensitivity, detection limit and quantification limit.

Chapter 2

Theoretical Background

In this chapter a brief review is presented of the fundamental definitions of materials used and techniques applied. In the second part, a literature review of the most important works in biosensors based on carbon nanotubes and titanium dioxide nanostructures for H₂O₂ detection is presented.

2.1 What are Nanomaterials?

Nanomaterials (NMs) are materials where one of its dimensions is between 1 to 100 nm¹⁷. NMs are well-known to show astonishing and unique properties. Respect to bulky materials, same composition NMs differ from optical, mechanical, electrical, thermal and magnetic properties. Nanomaterials can be classified according their dimensionality as: zero-dimensional (0D), one-dimensional (1D) and two-dimensional (2D)¹⁸:

- Zero-dimension: All its dimensions are between 0-100 nm. These materials include quantum dots, atomic clusters, and nanoparticles.
- One-dimension: Only one dimension is larger than nanometric scale, the length is much larger than width. 1D materials include nanotubes, nanowires and nanofibers.
- Two-dimension: Two dimension are larger than nanometric scale. These materials include nanosheets, nanofilms and nanoribbons.

2.1.1 Carbon Nanotubes

Carbon nanotubes are one dimensional nanomaterials consisting in graphene layers rolled-up with nanometric diameters and lengths of many microns. Carbon nanotubes structure is based in a hexagonal lattice of graphene¹⁹. There are two types of CNTs: single-walled carbon nanotubes (SWCNTs) and multi-walled carbon nanotubes (MWCNTs). SWCNT (Figure 2.1, left) consists in a single graphene cylinder whereas MWCNT (Figure 2.1, right) consists in two or more concentric cylindrical graphene sheets. Also, depending on their rolling angle, nanotubes are classified on three chiralities: armchair, zigzag and chiral one²⁰.

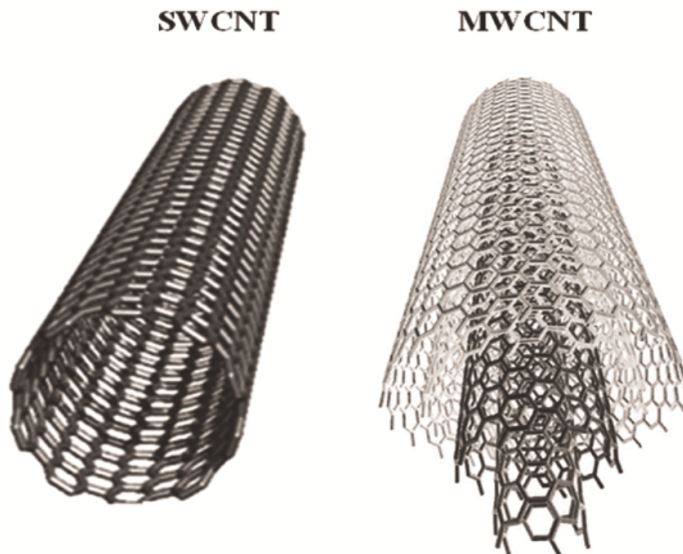


Figure 2.1: Diagrams of (left) a single-walled carbon nanotube and (right) a multi-walled carbon nanotube.¹

The hexagonal lattice of graphene arises because of the sp_2 hybridization of carbon atoms⁴. Each carbon atom is connected to other three atoms, while a free electron delocalized in the p_z orbital moves along an electron cloud²¹. The free delocalized electrons are the reason of the high electron conductivity. This electron cloud leads to substrate adsorption as result of $\pi - \pi$ interactions²². Also, surface functionalization of CNTs through chemical methods insert functional groups or effects which improve the chemical compatibility to substrates²³.

2.1.2 Titanium Dioxide

Titanium dioxide is a semiconductor material which occurs in three crystalline phases: anatase, rutile and brookite. Anatase and rutile are crystalline phases following a tetragonal system but brookite is orthorhombic²⁴. Titanium dioxide nanomaterials are commonly presented as nanoporous materials, nanosheets, nanotube arrays and nanoparticles²⁵. These materials present exceptional properties applied in areas as photocatalysis, photovoltaics, water and air purification, energy conversion and sensing^{11,26,27}.

Titanium dioxide nanostructures are synthesized with different methods as sol-gel, hydrothermal, CVD, PVD methods to mention a few²⁵. Sol-gel is a method based on an acid-catalyzed hydrolysis and polymerization of a titanium precursor to form a colloidal suspension²⁵, which let the formation of nanosized structures at relatively low temperatures with a high purity and homogeneous composition²⁸.

2.2 Biosensors

A biosensor is a device that measures a variation of electrical signal produced by a chemical or biological reaction. This signal is proportional to the analyte concentration and provides quantitative information about the analyte²⁹. The wide range of applications of biosensors include monitoring, food industry, fermentation processes, health field and metabolic engineering³⁰. A common biosensor is represented in Figure 2.2, consisting in the following components:

The **analyte** is the substance of interest in the detection, in this case, hydrogen peroxide. The **bioreceptor** is the component to which the analyte attaches. The recognition between the analyte and bioreceptor generates the chemical signal due to the reaction. The **transducer** transfers the output signal to an electrical signal. The process of conversion is called signalization. The transducer is also called electrode or detector. This electrical signal finally reaches the **electronics** and a display which amplifies the signal and converts it to a digital signal⁸.

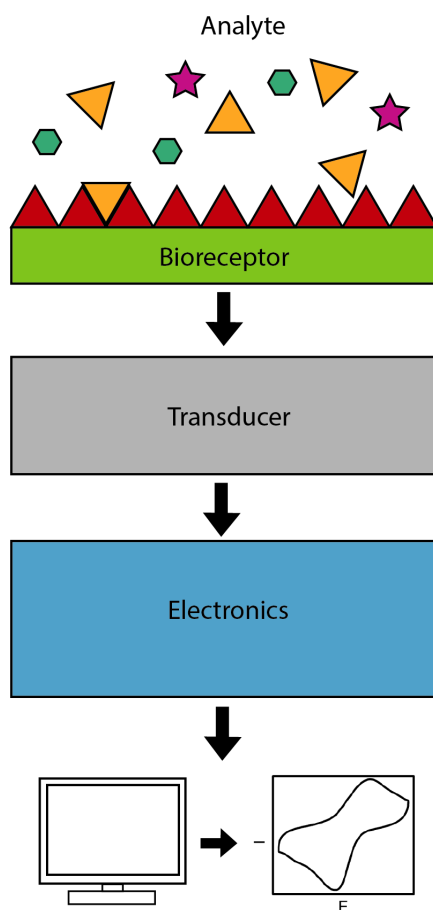


Figure 2.2: Scheme of components of a biosensor.

2.2.1 Nanomaterials in Biosensors

Regardless the novel properties of nanomaterials in their electronic and physical properties, nanomaterials also exhibit different chemical properties due their ability to accept or donate charges¹⁸. Studies^{31–33} have shown the ability of nanomaterials to provide an immobilization site for the bioreceptor due to their high surface area. Besides nanomaterials afford an enhancement of electron transport, acting as mediators, between the receptor and the surface electrode³⁴.

The enzyme immobilization and electrode modification occur via two basic ways: physisorp-

tion and chemisorption. a. Physisorption or physical adsorption refers to conjugation of deposited layers through electrostatic interactions³⁵. The different charges that nanomaterials and enzymes present lead to attachment stability. It is a simple fast method, but it does not take into consideration about favorable orientations (in case of enzymes), decreasing activities. b. Chemisorption is a specific procedure which involves the covalent interaction between the enzyme, the nanomaterial and the electrode surface³⁵. This method must be developed in a specific way that do not compromise the stability of the enzyme; for example, some authors commonly include thiol groups to attach enzymes or biomolecules to the electrode surface^{8,34}.

2.3 Prussian Blue and its Catalytic Activity

Prussian Blue (PB) or ferric hexacyanoferrate is a polycrystal with a face centered cubic lattice with a cell constant of 10.2 Å³⁶. Figure 2.3 shows Prussian Blue molecule. It is known from ancient times of dyeing applications due its deep blue color, but Neff³⁷ discovered its electroactivity with the formation of thin layers over electrodes surfaces. Prussian Blue is synthesized by mixing iron ions of different oxidation state forming a blue colloid, while its electrodeposition can be achieved with equimolar ferric-ferricyanide mixtures at 0.4 V applied voltage. The precipitation is given according the reduction of Fe⁺³ to Fe⁺² ions over the electrode surface³⁸.

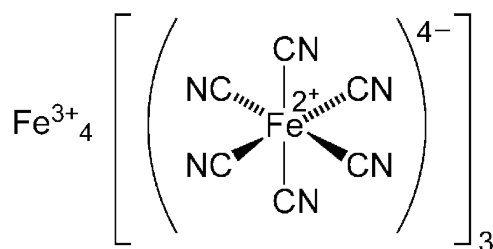
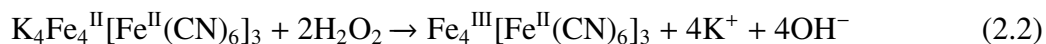


Figure 2.3: Prussian blue molecule

Applications of Prussian Blue varies from sensors for non-electroactive cations to sensors for oxidizable compounds and detection of hydrogen peroxide. PB has been reported to reduce and oxidize hydrogen peroxide. Reduction of hydrogen peroxide is catalyzed by the divalent iron ion Fe⁺², centers in the Prussian Blue molecules³⁶ by a two-electron reduction. Karyakin³⁹ proposed

the reaction of the reduction of H₂O₂ catalyzed by Prussian Blue as:



2.4 Quantitative Measurement

Three important parameters are considered for quantitative measurement:

Sensitivity means how the variation in analyte concentration produces a change in the current signal. It is the slope in the calibration current.⁴⁰

Limit of detection (LOD) refers to the smallest amount of analyte detectable with the electrode. LOD must reach a confidence level respect to the blank signal. The detection limit is commonly expressed as⁴⁰:

$$\text{LOD} = \frac{3 \cdot \text{SD}_{\text{blank}}}{s} \quad (2.4)$$

where SD is the standard deviation of N replicated measurements of the blank and s is the slope of the calibration curve. Even if the analyte is detected at concentrations near to LOD, the precision is questionable due to no proportional responses.

Then, the Limit of Quantification (LOQ) is the smallest analyte concentration that is possible to quantify. Quantification limit is stated as⁴⁰:

$$\text{LOQ} = \frac{10 \cdot \text{SD}_{\text{blank}}}{s} \quad (2.5)$$

2.5 Electrochemical Techniques

The electrochemical techniques used in this research were:

2.5.1 Cyclic Voltammetry

Cyclic voltammetry is an electroanalytical technique to study electroactive species and its redox behaviour over a selected potential range. The specific potential range is cycling over the potential of an electrode to measure the current response⁴¹. It is also used to study electron transfer-initiated chemical reactions. The results of CV are well predicted by Nernst equation (Equation 2.3).

$$E = E^0 + \frac{RT}{F} \ln \frac{(Ox)}{(Red)} \quad (2.6)$$

The results from a CV is called a voltammogram, where the x-axis represents the applied potential (E), and the y-axis is the current response (i). Figure 2.4 shows that applied potential scanned positively from point A to B is called *forward scan* and it occurs in certain time *t*. After the system reaches B, the potential starts to go reverse to the initial potential (from point B to C) and it is called *reverse potential*. Note that E initial and E final are the same.

The rate at which the potential is changing is called scan rate. It describes how fast is the variation of the applied potential. Slower scan rates lead to an increment in the size of the diffusion layer. For a reversible electron transfer process in a redox species, Randles-Sevcik equation (Equation 2.4) describes how the peak current (*i_p*) changes linearly with the square root of the scan rate *v* (V s⁻¹). This equation can give us information whether an analyte is freely diffusion in solution⁴²:

$$i_p = 0.4463nFAC \left(\frac{nFvD}{RT} \right)^{\frac{1}{2}} \quad (2.7)$$

where *n* is the number of electrons transferred in the redox event, *F* is the Faraday's constant, *A* is the electrode area, *C* is the concentration of the redox specie, *D* is the diffusion coefficients, *R* is the gas constant, *v* is the scan rate and *T* is the temperature in K.

2.5.2 Chronoamperometry

It is a technique where the electrochemical cell is subjected to a change in the voltage steps to measure the continuous current change response as function of time. The stepped voltage occurs at the working electrode. It is a common technique, inside the called *Pulsed techniques*, used for

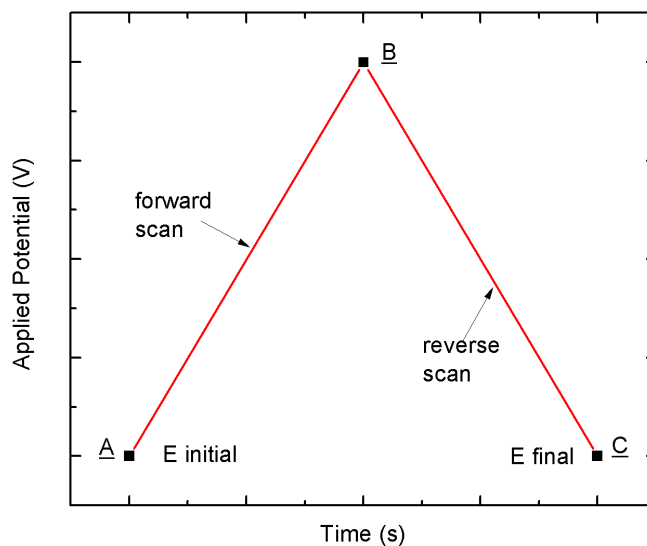


Figure 2.4: At initial t_0 starts from point A and finishes at point C returning to the same potential value.

controlled electrolysis or electrodeposition. The potential is applied with a fixed pulse while the current is measured as function of time as displays Figure 2.5. The stepped potential depends on the reduction potential of the analyte, which can be determined performing a cyclic voltammety sweep. In this work, chronoamperometric technique is used to electrodeposit a layer of Prussian Blue over the modified electrode⁴³.

2.5.3 Zeta Potential

Zeta potential (ζ) or potential at liquid-solid interface is a characterization technique based on the double layer interaction of a solute and its solvent⁴⁴. The technique measures the electrostatic potential at the interface of the ions in the diffuse layer and the bulk dispersing ions⁴⁵ as indicate Figure 2.6. This potential is closely related with the surface charge of the particle and it is key to control electrostatic interactions in a dispersion. The potential distribution itself determines the

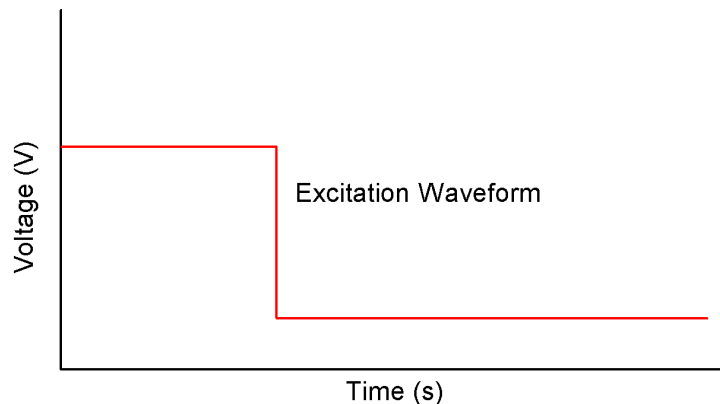


Figure 2.5: Chronoamperometry excitation waveform of voltage along time

interaction energy between the particles, responsible for the particle stability⁴⁶.

Zeta potential technique is based in Electrophoresis Light Scattering (ELS). The sample solution is irradiated by a beam. The beam is, consequently, scattered by the particles causing a frequency shift. The frequency shift will depend on the electrophoretic mobility of the particles. The zeta potential is calculated from the electrophoretic mobility using the Henry Equation (Equation 2.5)⁴⁵:

$$U_e = \frac{2\epsilon\zeta f(\kappa a)}{3\eta} \quad (2.8)$$

where U_e is the electrophoretic mobility, ϵ is the dielectric constant, $f(\kappa a)$ is the Henry function, κa is a particle radius measurement and η is the absolute zero-shear viscosity of the medium⁴⁵.

2.5.4 Amperometry (i-t Curve)

Amperometry is a technique that measures of current variation at a fixed potential. The variation of current is proportional to the analyte concentration in contact with the electrode surface, while the applied potential is the driving force of the oxidation or reduction of the analyte⁴⁰. If oxidation is occurring, the analyte will lose electrons which will travel to the surface electrode and will

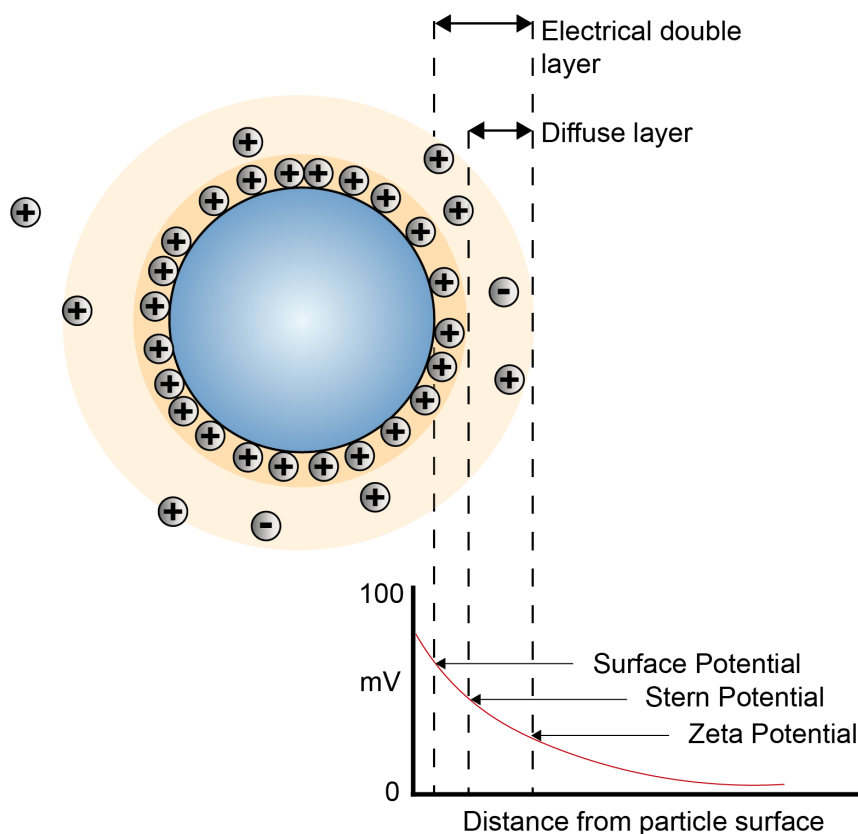


Figure 2.6: Scheme of the electrochemical double layer at the solid-liquid interface displaying the potential as function of particle-ion distance

be measured as current variation by a potentiostat. It happens in the opposite way with analyte reduction. The amperometric determination depend on Faraday's law (Equation 2.6):

$$Q = nFN \quad (2.9)$$

where Q is the charge (coulombs) necessary to reduce/oxidize N moles of analyte, n is the electron number involved in the transfer process and F is Faraday's constant. Deriving Equation 2.6 respect to time, it yields the current measured (Equation 2.7)⁴⁰:

$$\frac{dQ}{dt} = I = nF \frac{dN}{dt} \quad (2.10)$$

The current response is commonly plotted as function of time. As amperometry is a surface technique, the analyte molecules must be forced to reach the electrode surface to be oxidized or reduced. This molecule movement is reached with constant stirring of the solution.

2.6 Literature Review

The following section gives an overview of the literature related to the design of biosensors based on carbon nanotubes, titanium dioxide and specifically, for hydrogen peroxide detection.

Historically, the first biosensor was developed in 1956 by Leland Clark for oxygen detection. Since then, the development of biosensors was rapidly increasing, following for amperometric enzyme-based biosensors until the first commercial biosensor was developed by Yellow Spring Instruments in 1975⁴⁷. From a few years ago, research has focused in the use of nanomaterials to improve biosensors due the exceptional properties they exhibit.

2.6.1 Carbon Nanotubes-based Biosensors

The architecture of carbon nanotube-based biosensors relies on the different configuration of electrode assemble. Some proposals of CNT-based biosensor are summarized below:

Liu⁴⁸ immobilized glucose oxidase (GOx) in a carbon nanotubes and chitosan matrix enhancing the electron transfer rate of the enzyme to 7.73 s^{-1} . The composite was prepared in a single composite of chitosan in acetic acid, carbon nanotubes and the enzyme. It exhibited the ability to maintain the bioactivity of GOx and higher sensitivity and stability after 50 cycles. The presence of a N_2 -saturated solution helps out the in the catalytic activity of GOD giving a higher signal compares than air or O_2 -saturated solution.

An amperometric biosensor for hydrogen peroxide was developed by Qian and Yang⁴⁹. The biosensor was enzyme-based, using horseradish peroxidase (HRP). The electrode was modified with a composite of MWCNTs and chitosan, glutaraldehyde and HRP. The activity of HRP was studied via cyclic voltammetry and amperometric techniques in phosphate buffer solution pH 7.

The electrode modification showed a good electrocatalytic activity and stability. The electrode stability may be due to the enzyme immobilization to due cross-linking by glutaraldehyde leading its active center disposed to H_2O_2 detection. In another reference, Besteman⁵⁰ studied the redox glucose oxidase behaviour immobilizing the enzyme onto the sidewalls of single-wall CNTs. The conductance of the system has been affected after the immobilization of the enzyme due to the proposal of a variation in capacitance change rather than electrostatic interactions. The presence of glucose oxidase adhered to the walls of SWCNTs inhibits the ions of the electrolyte to completely interact with the carbon nanotube and it leads to the decreasing of the gate capacitance and therefore, a decreasing on the total capacitance.

2.6.2 TiO_2 & TiO_2 /Carbon Nanotubes-based Biosensor

Titanium dioxide is well-know as a semiconductor with photocatalytic properties and biocompatible material. Fotouhi⁵¹ prepared a nanocomposite based on TiO_2 NPs/MWCNTs in a chitosan matrix for simultaneous determination of dihydroxybenzene isomers: hydroquinone, catechol and resorcinol. It is quite clear to see the signal enhancement in voltammograms of the bare GCE compared with the nanocomposite. The electrode showed a slightly decrease in the electrochemical response after 48h, indicating a long-term stability.

A glucose biosensor based on titanium dioxide/carbon nanotubes-chitosan is being reported by Zhang⁵². The addition of a layer of Prussian Blue acted as mediator for catalyst H_2O_2 reduction for lower potentials. A poly(diallyldimethylammonium chloride) (PDDA) layer was also added to a glassy carbon electrode to enhance the electrostatic stability of the layers. The PDDA layer was doped with gold nanoparticles to increase the electrical conductivity of the modified electrode. It displayed a low relative standard deviation (1.2%). The layered system provided a efficient maintenance of the enzyme and keep its enzymatic bioactivity. It also exhibited a linear range from $6\mu\text{M}$ to 1.2 mM with a detection limit of $0.1\mu\text{M}$.⁵²

A biosensor based on TiO_2 nanotubes arrays modified with a thin Au for H_2O_2 detection was designed by Kafi⁵³. Horseradish peroxidase was immobilized along a chitosan matrix over the Au-modified TiO_2 nanotube arrays. According to the evaluation, the Au film plays a

crucial role in electron transfer. The amperometric response of the electrode showed long-range linearity and stability. Shen⁵⁴ doped carbon paper with a TiO₂/CNTs nanocomposite for cancer cells detection. TiO₂ were grown over CNTs using the sol-gel method. The electrochemical characterization indicates that the redox electron transfer is a diffusion controlled process and leads to an enhancement of the sensitivity. The treatment with cancer cell exhibited an increasing in the electrochemical response which brings the possibility for biomedical applications.

Chapter 3

Methodology

3.1 Electrochemical Equipment

3.1.1 Reagents and Solutions

The electrode polishing treatment was carried with 0.1 M nitric acid (HNO₃) solution. The 0.1 M HNO₃ solution was prepared by dissolving 6.33 mL in 1000 mL of distilled (DI) water. Carbon nanotubes dispersion was prepared in a 5 mg/mL concentration regardless the carbon nanotubes sample, or used solvent. For H₂O₂ detection, Sigma-Aldrich Hydrogen peroxide solution 30 % (w/w) in H₂O ($\delta= 1.110 \text{ g/cm}^3$) was used. For all the washing, rinsing and preparation of solutions, DI water was used.

0.1 M Phosphate Buffer solution pH 7

The support electrolyte used for the electrode characterization and peroxide detection was phosphate buffer pH 7. The 0.1 M phosphate buffer solution (PBS) pH 7 was done by preparing 0.1 M potassium phosphate monobasic solution dissolving 3.4 g of KH₂PO₄ in 250 mL and 0.2 M sodium hydroxide solution by dissolving 0.8 g of NaOH in 100 mL. Then, mix 250 mL of KH₂PO₄ solution with 73 mL of NaOH solution and complete to 500 mL.

4 mM Potassium Ferricyanide solution

The reaction kinetics of an electrode is commonly characterized with a ferricyanide solution due to its ideal redox behavior. A 4 mM $\text{K}_3[\text{Fe}(\text{CN})_6]$ solution was prepared by dissolving 32.92 mg of potassium ferricyanide in 25 mL of PBS at pH 7.

Prussian Blue solution

The Prussian Blue deposition was carried out with a solution based on the mixture of equimolar potassium ferricyanide and iron (III) chloride solutions. A solution of 2.5 mM $\text{K}_3[\text{Fe}(\text{CN})_6]$ was prepared by dissolving 20.58 mg of potassium ferricyanide in 25 mL of DI water, while the 2.5 mM FeCl_3 was prepared by dissolving 16.9 mg of ferric chloride in 25 mL of DI water. The mixture is dissolved in 0.1 M KCl and 0.1 M HCl as supporting electrolytes.

3.1.2 Electrochemical Cell and Electrodes

The electrochemical cell used in all the experiments was a standard three electrode system with a single compartment. Every experiment was carried out with 25 mL of solution. The three electrodes used in the cell were: a glassy carbon electrode (working electrode), Ag/AgCl electrode (reference electrode) and graphite electrode (counter electrode). In the cell, the separation distance of the working electrode and reference electrode was designed to be the shortest possible, about 1 centimeter.

Glassy Carbon Working Electrode

BASi MF-2012 Glassy Carbon Electrode (GC) was used in all the experiments. The active disk of the electrode has a 3.0 mm diameter while its plastic body is 7.5 cm length x 6 mm OD, which is solvent-resistant.

Silver-Silver Chloride Reference Electrode

The reference electrode was a commercial CHI 111 Ag/AgCl from CH Instruments, Inc. The internal saturated solution is 1 M KCl of filling.

Graphite Counter-Electrode

A commercial graphite bar of 1cm diameter was used as counter-electrode. Its intrinsic conductive property was ideal to let the current flow.

3.1.3 Hardware and Software

All electrochemical techniques were performed in an Autolab PGSTAT302N high current potentiostat/galvanostat equipped with the FRA32M impedance spectroscopy module. All the techniques were run in the Nova 2.1 Metrohm Autolab software. The data is analyzed and the presented graphs are plotted in OriginPro 8.0.

3.2 Nanostructures Synthesis

3.2.1 Functionalization of Carbon Nanotubes

Pristine multi-walled carbon nanotubes (pCNTs) were obtained from Nanocyl S.A. pCNTs were subjected to a prefunctionalization and functionalization process. To perform this work, the materials were obtained already prefunctionalized and modified with TiO₂ NPs. A brief description of the process is given below.

Pre-functionalization process was performed with 3M HNO₃ and 1M H₂SO₄ solutions. pCNTs were dissolved into the nitric acid solution while the sulfuric acid solution was slowly added. The solution was placed under reflux process at 80°C and stirring of 400 rpm for 6 hours. Then, the nanotubes were filtered, rinsed, dried (12h) and finally, grinded with pestle in a mortar.

The functionalization process caused the addition of carboxylic and hydroxyl groups to the nanotubes surface. These groups were added to improve the compatibility with substrates and the media. The procedure was done adding 60% w/w HNO₃ solution to pre-functionalized CNTs and submitted under sonication and stirring of 400 rpm at 80° C for 2 hours. The final suspension was filtered, rinsed and dried (16h). The resultant nanotubes were milled in a mortar and sieved with a 125 μ m sieve.

3.2.2 Synthesis of TiO₂-CNT Nanostructures

The synthesis is based on the sol-gel technique using the previous functionalized carbon nanotubes (fCNTs) (150.0 mg), titanium isopropoxide as precursor (0.6 mL), isopropanol as solvent (18.2 mL), acetic acid and deionized water. The fCNTs were suspended into the half volume of isopropanol and sonicated for 30 minutes. A solution of titanium precursor and quarter volume of isopropanol was prepared. The solution was dropped out over half volume of fCNTN suspension with constant stirring of 600 rpm. Then, a solution of left isopropanol and deionized water was sonicated for 10 minutes and dropped to the main solution. The reaction was continued over the same parameters of stirring and temperature for 2 hours. The suspension was left to age for 20 days at room temperature. The solvent was evaporated at 80-88°C and washed three times with deionized water letting it to evaporate. The resultant precipitate was dried up under vacuum at 80°C for 4 hours, followed by a thermal treatment at 500°C in Ar atmosphere for 2 hours. The final substance was milled to obtain a thin powder.

3.3 Characterization of Carbon Nanotubes

3.3.1 Transmission Electron Microscopy

The TEM images were obtained in a JEOL 1220 microscope of Polymers Laboratory of Simon Bolivar University (Venezuela) with an accelerating voltage of 100kV. The samples were prepared using a wet suspension technique with an ethanol/water (70% v/v) solution.

3.3.2 Fourier Transform Infrared Spectroscopy

The spectra were performed in a Nicolet iS10 FTIR spectrometer in Chemistry Center of IVIC. The samples were prepared in KBr pills. The frequency range of spectra goes from 4000 to 400 cm⁻¹ with 64 sweeps at 2 cm⁻¹ resolution.

3.3.3 X-Ray Diffraction

The samples were analyzed via a SIEMENS D5005 diffractometer with a wavelength of 1.54178 Å and a range of $2\theta = 10^\circ$ to 80° with a rate of 0.02°/0.52 s. The data were collected from

Laboratory of Environmental Chemistry of IVIC, Venezuela.

3.3.4 Zeta Potential

Zeta potential technique was performed over both samples of nanotubes (fCNT and TiO₂-CNT). The measurements are done in an aqueous suspension of carbon nanotubes samples with distilled water as the solvent. The environment conditions of the analysis area were a temperature of 24.1° and a humidity of 45.7%. Both samples were submitted to 5 runs of measure. From this data, we will be able to calculate the mean and standard deviation values from the zeta potential and half width of the peaks. This test was performed at Escuela Politécnica Nacional, Quito, Ecuador.

3.4 Electrode Modification

3.4.1 Electrode Polishing

The glassy carbon surface is highly reactive, and impurities or different modifications could result in variations in its electrochemical activity⁵⁵. These variations rely on the starting electrode surface. The most common electrode pretreatment to acquire reliable results is polishing. The polishing treatment removes the impurities and residues of the glassy carbon surface. The CHI glassy carbon electrode of this work went through a polishing treatment each time it had been modified. The treatment consists in two process: an alumina (1) and an electrochemical polishing (2).

1. Glassy carbon surface was polished with a polishing cloth in an aqueous slurry of 1 μm, 0.3 μm and 0.05 μm alumina powder performing eight-like moves for 5 minutes. After the cleaning, the electrode was rinsed with distilled water.
2. GCE is assembled in a three-electrode cell containing 25 mL of 0.1 M of nitric acid (HNO₃). The electrode was submitted to 50 cyclic voltammetry cycles from -1 to 1 V with a scan rate of 100 mV/s with a negative initial polarization.

3.4.2 Dispersion of Carbon Nanotubes

Functionalized CNTs and TiO₂-CNTs were characterized via zeta potential to observe the superficial charge (See Results Discussion: Zeta Potential). fCNTs displays a strong cationic behavior due the presence of -COOH and -OH groups, while TiO₂-CNT exhibit a slight anionic behavior. Both samples were dispersed in different solvent.

Functionalized CNT were dispersed in dimethylformamide (DMF) in a concentration of 5mg/mL, while TiO₂-CNT were suspended in sodium dodecyl sulfate (SDS) at the same concentration as above. Both suspensions were placed in 1.5 mL tubes and sonicated for 10 minutes.

For TiO₂-CNT modified electrode, an equal-concentration suspension is made of 5 mg/mL of TiO₂/CNT in 1% sodium dodecyl sulfate solution (SDS). The SDS solution is made by dissolving 10 mg of SDS per mL of distilled water. Sonication is applied to the mixture for 15 minutes.

3.4.3 Modification of PDDA/CNT/GC Electrode

The glassy carbon electrode must be previously polished with the treatment explained above: alumina and HNO₃ polishing, and then washing with distilled water and drying to room temperature.

After the electrode is completely dried, a suspension of carbon nanotubes (CNT) of a volume of 10 μL was pipetted onto the electrode surface. The suspension droplet must be uniformly dispersed over the electrode surface. The electrode was dried at 50° C for 15 minutes. Then, 10 μL of PDDA solution was pipetted into the CNT modified-electrode surface and dried at 50°C for 15 minutes. The suspension droplet must be uniformly dispersed over the electrode surface.

3.4.4 Modification of PDDA/TiO₂-CNT/GC Electrode

The following modification of the electrode with TiO₂-CNTs is carried out with almost the same procedure as for CNTs sample. The difference is that PDDA is not deposited over the nanotubes layer. This is due to the different surface charge the TiO₂-CNTs exhibit.

3.4.5 Electrodeposition and Activation of Prussian Blue

After the two-layer dropping, a Prussian Blue (PB) layer is deposited via chronoamperometry (CA) technique.

An aqueous solution of 24 mL is prepared in equal volumes of 6 mL of 0.1 M KCl, 0.1 M HCl, 2.5 mM $K_3[Fe(CN)_6]$ and 2.5 mM $FeCl_3 \cdot 6H_2O$. KCl and HCl acted as supporting electrolytes. The electrodeposition was done immersing the modified electrode in the solution and applying 2 pulses of constant potential of 0.4 V by 60 seconds using CA³⁹.

After the deposition, the PB layer was activated with cyclic voltammetry with 12 mL of 0.1 M KCl and 12 mL of 0.1 M HCl as supporting electrolytes. The activation was applying 20 cycles in a potential range of -0.2 to 0.8 V at a scan rate of 50 mV/s. The electrode is dried up at 50°C for 15 minutes. A final layer of 10 μ L of PDDA is pipetted over the electrode surface and dried at 50°C for 15 minutes.^{52,56} The final electrode arrangement is doubled rinsed with distilled water.

The whole modification process of the electrode is summarized in the Figure 3.1.

3.4.6 Peroxide Detection

The detection was achieved using hydrogen peroxide solution 30% (w/w) in H_2O with two different techniques: cyclic voltammetry and chronoamperometry.

Via Cyclic Voltammetry

The catalytic activity of Prussian Blue over hydrogen peroxide was evaluated varying the H_2O_2 concentration and recognizing the redox peaks response. The detection was carried out in different concentrations from 0.5 μ M to 4.0 μ M. A 0.1 M H_2O_2 solution was prepared by dissolving 255.1 μ L in 25 mL of deionized water. From this solution, less concentrated solutions were prepared according Table 3.1.

Once the solutions were prepared, they were refrigerated at 10 °C. One by one (starting with the less concentrated solution), they were placed into the system and 2 sweep segments of cyclic voltammetry were performed. The parameters are summarized in Table 3.2.

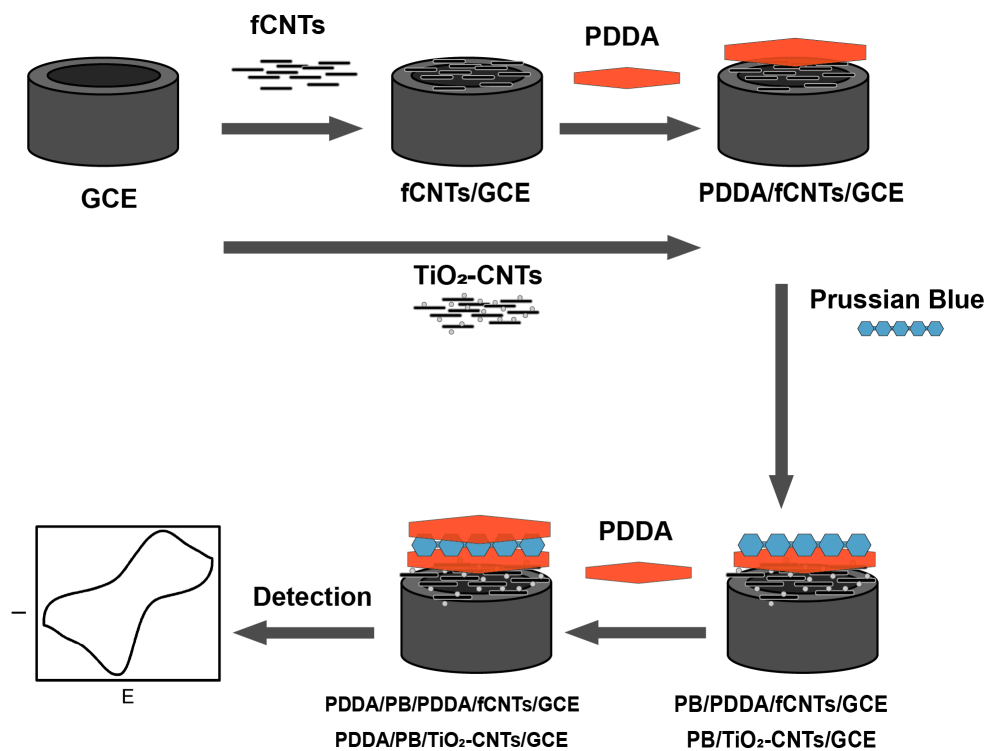


Figure 3.1: Scheme of PDDA/PB/PDDA/TiO₂-CNTs/GC electrode modification.

[H ₂ O ₂] (mM)	V _{0.1MH₂O₂} (μL)	Left to 1 mL of PBS (μ L)
1.0	250	750
1.5	375	625
2.0	500	500
2.5	625	375
3.0	750	250
3.5	875	125
4.0	1000	0

Table 3.1: Quantities of reactives to prepare 25 mL H₂O₂ solutions from 1 mM to 4 mM

Via Amperometric I-t Curve

The steady-state current response of H_2O_2 with the modified electrode was evaluated through amperometric I-t curve. This technique consists in adding aliquots of a known concentration stock solution over the electrochemical cell fullfilled with an electrolyte solution, and measure the change in current signal as the cell concentration varies. These response was based on the reduction of H_2O_2 from the electrocatalysis of Prussian Blue; so, 0 V was selected as the applied potential for the detection.

A stock solution of 0.1 M H_2O_2 was prepared by dissolving 102 μL in 10 mL of distilled water. Each aliquot was selected to be 100 μL of the stock solution added each 20 seconds. These H_2O_2 detection was carried out with both modified electrodes. In Table 3.3 is summarized the applied parameters.

3.5 Electrochemical Characterization

3.5.1 TiO_2 -CNTs and fCNTs/GCE Characterization

The electrochemical behavior of modified and bare electrodes was investigated on PBS pH 7 solution using cyclic voltammetry. The first experiment analyze the contribution of carbon nanotubes dispersion and the potential window each one modified electrode exhibit respect to bare glassy carbon electrode. The window potential refers to the electroactive range of potential of an electrode in a determined support electrolyte. The PBS preparation procedure is detailed in the subsection Reagents and Solutions. The modified electrode was immersed in 25 mL of PBS in the electrochemical cell. The CV was run over 20 cycles to reach stability of the electrode, that means, where the current response do not change over cycle.

The cyclic voltammograms were performed over the parameters shown in Table 3.4:

The reaction kinetics characterization uses potassium ferricyanide ($\text{K}_3[\text{Fe}(\text{CN})_6]$) is a typical electrochemical analysis to study the redox capability of the electrode. Potassium ferricyanide is used due to the nearly ideal reaction of the one-electron reduction of ferricyanide to ferrocyanide. This coupled reaction exhibits a reversible behavior with no subsequent reactions. This charac-

Technique:	Cyclic Voltammetry
Parameter	Value
E_0	0.6 V
E_h	0.6 V
E_l	-0.6 V
Initial Polarization	Negative
Scan Rate	50 mV/s
Sample Interval	0.001 V
Quiet Time	5 s
Sensitivity	0.001 A/V

Table 3.2: Parameters to evaluate the presence of hydrogen peroxide via cyclic voltammetry in a 25 mL PBS pH 7

Technique:	Amperometric i-t Curve
Parameter	Value
$E_{initial}$	0.5 V
Sample Interval	0.2 s
Run Time	500 s
Quiet Time	5 s
Sensitivity	1×10^{-5} A/V
Aliquot	100 μ L of 0.1 M each 20 s

Table 3.3: Parameters to measure the amperometric response of the sensor to hydrogen peroxide through successive injections of 0.1 M H_2O_2 in 20 mL of PBS

Technique:	Cyclic Voltammetry
Parameter	Value
$E_{initial}$	0 V
E_{high}	1.9 V
E_{low}	- 1.9 V
Quiet Time	5 s
Sensitivity	1×10^{-3} A/V
Scan Rate	100 mV/s

Table 3.4: Parameters of cyclic voltammetry over bGCE, PDDA/fCNT/PDDA/GCE and PDDA/TiO₂-CNT/GCE in 25 mL of PBS pH 7

terization was performed using CV under the variation of the scan rate with the parameters shown in Table 3.5.

The characterization was done immersing the electrodes in a 4 mM ($K_3[Fe(CN)_6]$) solution. The ferricyanide was dissolved in PBS, which acts as supporting electrolyte.

3.5.2 Prussian Blue-modified GCE Characterization

After the last PDDA layer was placed and the whole modification is complete, the PDDA-PB-PDDA-xCNT-GC electrode is characterized via the redox peaks the Prussian Blue exhibits. The reaction kinetics of PB was done on 25 mL of PBS under the following parameters (Table 3.6).

Technique:	Cyclic Voltammetry
Parameter	Value
$E_{initial}$	0
E_{high}	0.5 V
E_{low}	- 0.5 V
Quiet Time	5 s
Sensitivity	1×10^{-3} A/V
Scan Rate	20 - 120 mV/s

Table 3.5: Parameters of cyclic voltammetry over bGCE, PDDA/fCNT/PDDA/GCE and PDDA/TiO₂-CNT/GCE in a 4 mM potassium ferricyanide solution.

Technique:	Cyclic Voltammetry
Parameter	Value
$E_{initial}$	0
E_{high}	0.8 V
E_{low}	- 0.2 V
Quiet Time	5 s
Sensitivity	1×10^{-3} A/V
Scan Rate	20 - 120 mV/s

Table 3.6: Parameters in CV to analyze the reaction kinetics of Prussian Blue-modified electrodes in PBS.

Chapter 4

Results & Discussion

This section presents simultaneously the results with the discussion for each part. In this way, functionalized carbon nanotubes with hydroxyl and carboxylic groups are named fCNT and carbon nanotubes doped with titania nanoparticles are named as TiO₂-CNT. The results of the electrode modification will be managed as four different designations as the modification procedure is detailed above: TiO₂-CNT/GCE refers to the glassy carbon surface modified with TiO₂-CNT, fCNT/GCE is the one modified with functionalized CNTs, including the PDDA layer; PB/TiO₂-CNT/GCE is the electrode which includes the Prussian Blue layer and its final layer of PDDA; and PB/fCNT/GCE refers to the electrode modified with CNT, the Prussian Blue layer and both layers of PDDA. The electrode modifications and its designations are summarized in Table 4.1

First, it will be discussed the physical characterization of CNT samples through TEM, FTIR and XRD. Then, zeta potential characterization will be evaluated followed by the subsequent CNT dispersion analysis. The electrochemical characterization of the modified electrodes with TiO₂-CNTs and fCNTs will be investigated via cyclic voltammetry; and finally, the evaluation of peroxide detection via CV and amperometric response.

Electrode	Label	Layers
1	TiO ₂ -CNT/GCE	TiO ₂ -CNT
2	fCNT/GCE	PDDA
		fCNT
3	PB/TiO ₂ -CNT/GCE	PDDA
		Prussian Blue
		TiO ₂ -CNT
4	PB/fCNT/GCE	PDDA
		Prussian Blue
		PDDA
		fCNT

Table 4.1: Summary of the electrodes, layers and designation employed in the work

4.1 Physical Characterization of TiO₂-CNT and fCNT Nanostructures

Physical analysis was performed to understand the morphological variations and surface chemistry of the nanostructured systems. Transmission Electronic Microscopy (TEM) characterization study the morphology of carbon nanotubes and its modifications with titania NPs.

Figure 4.1 exhibits the TEM images of functionalized CNTs. The shades on different sections of the image and the apparent change of grey tone indicate the bundling of the nanotubes over themselves. The diameter mean value of fCNT is 5 ± 2 nm. In the literature, the value of wall separation distance of a MWCNT is around 0.34 nm^{57} , thus the nanotubes are around 4-10 layers. Figure 4.1 (right) exhibits a multi-walled carbon nanotube, where approximately four walls are appreciated with a diameter of 3 nm, supporting the previous calculation and the wall distance assumption.

TiO₂-CNT nanostructure morphologies are displayed in Figure 4.2. In these images, titanium nanoparticles are observed to be adhered over the nanotube surface. The adhesion of the NPs is

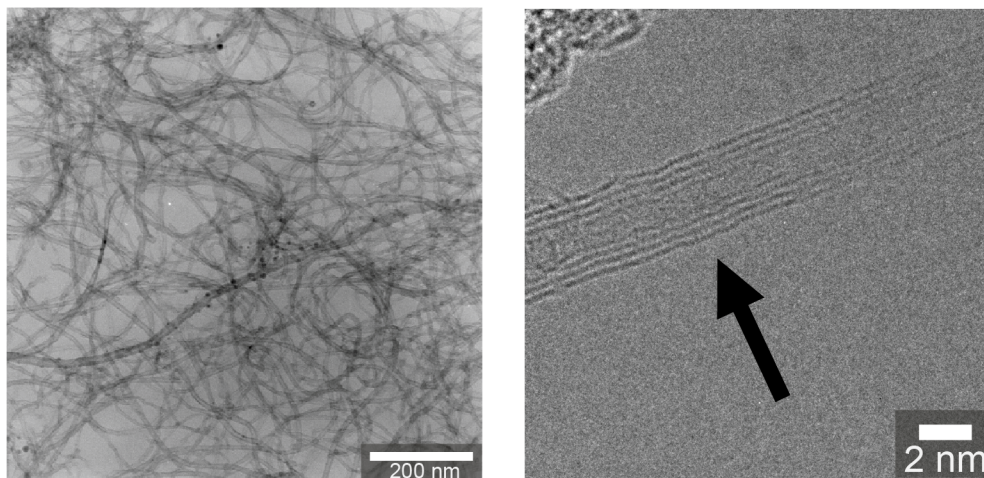


Figure 4.1: TEM images of functionalized carbon nanotubes.

assumed to occur mainly over the available functional groups from the previous functionalization; thus, NPs are not uniformly distributed over the nanotube surface. Nanoparticles tend to agglomerate over the surface with higher number of present functional groups and over the crossing of nanotubes as shown in Figure 4.2 (medium). The tendency to agglomeration is due to the high surface energy of titania nanoparticles of which did not bond to the nanotube; nevertheless, defined nanoparticles are still appreciated.

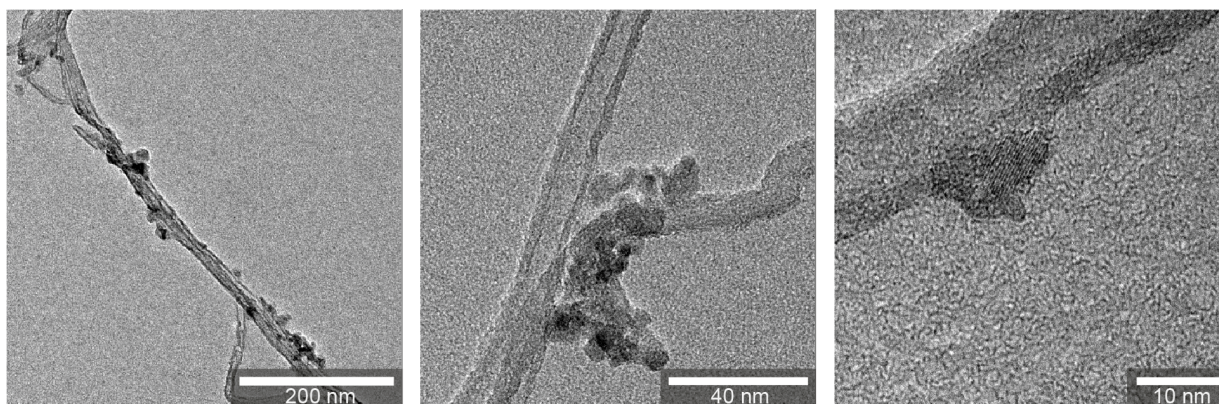


Figure 4.2: TEM images of TiO₂-CNT at different magnifications

Particle size of nanoparticles is measured from some TEM images given a mean value of 6.1 ± 1.3 nm. This value is close to the nanotube diameter.

XRD analysis are shown in the Figure 4.3 of TiO₂-CNT (a) and functionalized carbon nanotubes (b). fCNT spectra exhibits the characteristic peaks of graphite in nanotubes from the 002 and 100 planes. These peaks are in 26° and 43° , respectively. The 002 plane and its location indicate the interplanar distance of the nanotube layers. With $\theta_{002} = 26$ and according Bragg's law, the interplanar distance is 3.43 \AA . This calculation goes according to the previous assumption at the layers number calculation.

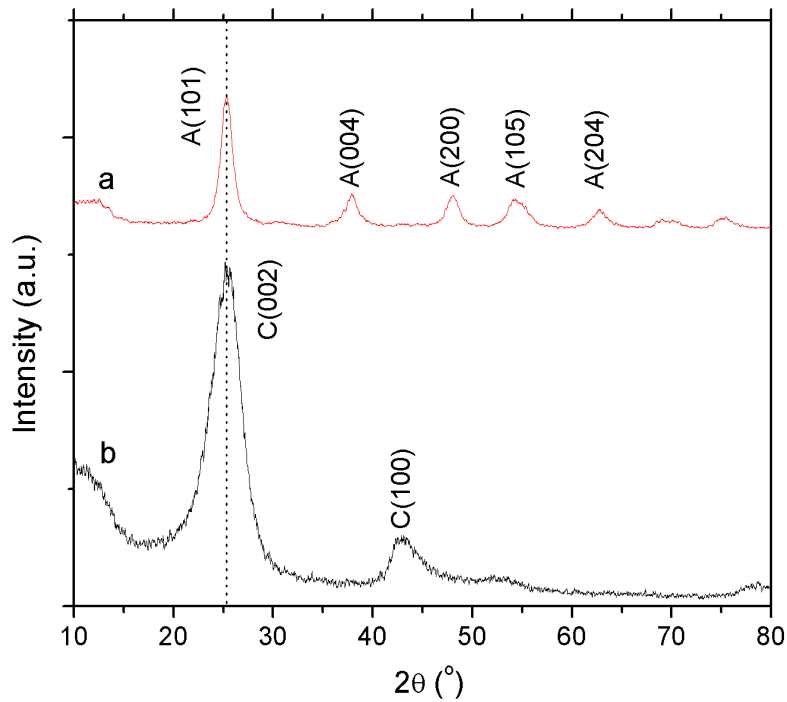


Figure 4.3: XRD diffractograms of (a) TiO₂-CNT and (b) fCNTs.

In TiO₂-CNT diffractogram, some peaks at 26° , 38° , 48° , 54° and 63° are present. Comparing these angles with the ones from the titanium phases; it is evident the peaks correspond

to the anatase crystalline phase and the angles agree with the (101), (004), (200), (105) and (205) planes, respectively⁵⁸. With Scherrer's equation⁵⁹, we conclude the diameter of the anatase nanoparticles is about 6.3 nm. This value is consistent with particle size measured from the TEM images. Qualitatively, the anatase peaks are shown to be broad which indicates the formation of crystals at nanometric scale. The main peak of 002 plane of CNT is not observed in the TiO₂-CNT spectra due to the overlapping with the 101 plane of anatase.

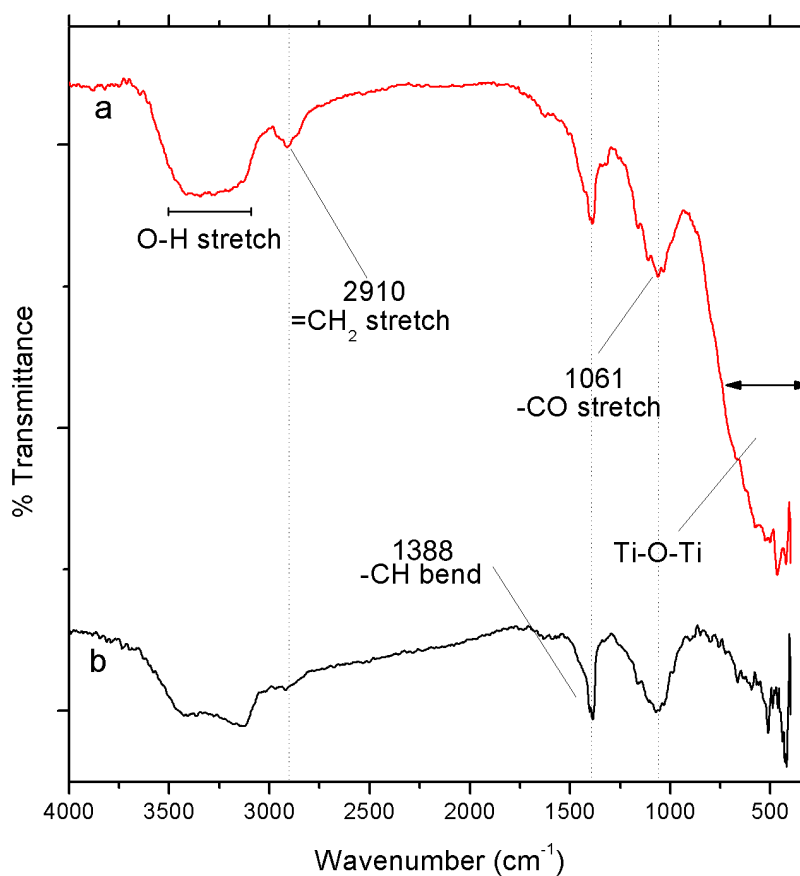


Figure 4.4: FTIR spectra of (a) TiO₂-CNTs and (b) fCNTs.

Complementing the physical characterization, Figure 4.4 shows the FTIR spectra of (a) TiO₂-CNT and (b) fCNTs in a range from 4000 to 400 cm⁻¹. As shown in the figure, TiO₂-CNT sample exhibits a band between 900-400 cm⁻¹. This band refers to the Ti-O-Ti bond and proves the presence of titania; while this band is absent in the fCNT spectrum. Additional peaks are present along the spectra in 3433, 3126, 1388, 1061 cm⁻¹. fCNTs spectrum exhibits a broad peak at 3280 cm⁻¹ which is a characteristic of the O-H stretching of hydroxyl group and refers to the oscillation of carboxyl groups⁶⁰, equivalent to the 3433 and 3126 cm⁻¹ peaks in the TiO₂-CNT spectrum. The peak at 2910 cm⁻¹ refers to the methylene stretching band assumed to be groups located at defect sites in the CNTs sidewalls⁶¹, while the 1388 cm⁻¹ peak could be attributed to rocking and bending of -CH group due to a possible hydrogenation in the functionalization process. The C-O bands are observed in both spectra at 1061 cm⁻¹, characteristic of carboxyl functional groups.

Functionalized CNT and TiO₂-CNT were characterized in a previous work by Albano⁶² via N₂ adsorption and BET area. In both cases, their results showed mesoporous structures with non-uniformed pore sizes independent on CNTs quantity. In the superficial area analysis, they showed an area of 298,40 ± 2.72 m²/g in the fCNTs, while for TiO₂-CNT, the area is 147.02 ± 1.89 m²/g. The presence of nanoparticles have reduced the superficial area of the sample respect the fCNTs, due to the coverage of the TiO₂ NPs on the CNTs walls.

4.2 Zeta Potential and Carbon Nanotubes Dispersion

Z-Potential characterization was done over the nanotubes samples, in order to analyze the charge over the electrical double layer. A potential difference is applied over the CNT suspensions to vary the mobility of the particles. This mobility will give information the charge they present. The applied potential is what controls the electrostatic interactions of the nanotubes and the solvent; and therefore, its colloidal stability⁶³.

Figure 4.5 is the curve of zeta potential of fCNTs in an aqueous solution. The mean value of zeta potential is -51.84 mV with a standard deviation of 9.66 mV, while Figure 4.6 is the plot of the zeta potential measured from the TiO₂-CNTs sample with a mean value of 9.93 mV with a standard deviation of 0.73 mV. The standard deviation values are calculated from five repeat

measurement over the same conditions on both samples.

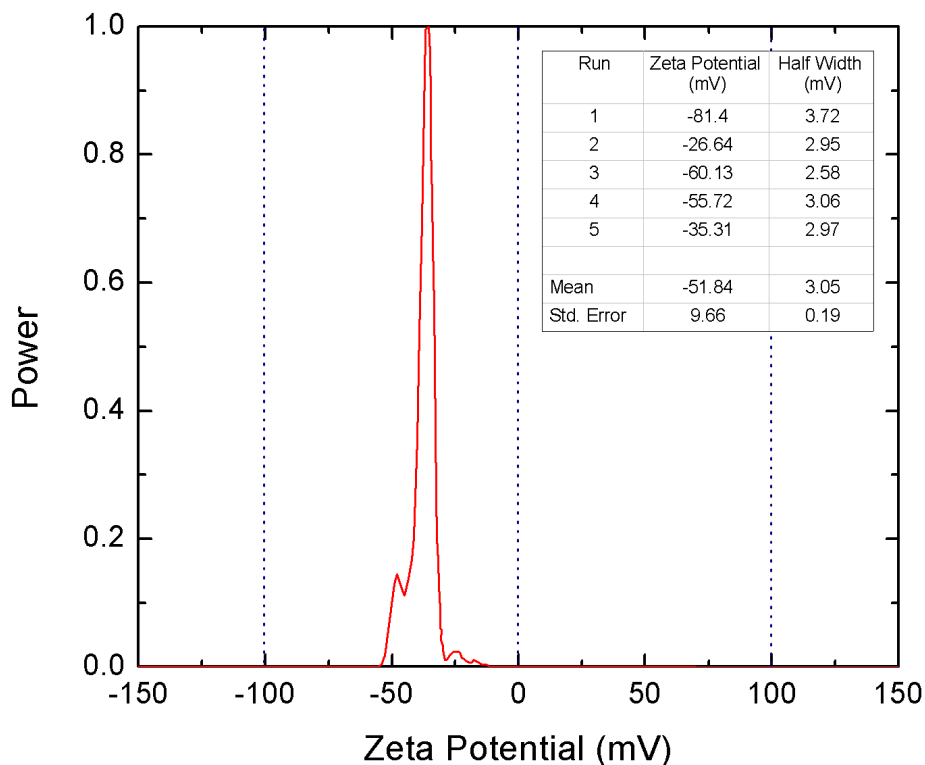


Figure 4.5: Zeta potential result for fCNTs showing a peak at -35.31 mV in the fifth run with a mean of -51.84 mV with a standard deviation of 9.66 mV.

In the functionalized CNTs, the previous acidic treatment over the pristine carbon nanotubes added carboxylic (-COOH) and hydroxyl groups (-OH) on their walls; so, the negative charge is due to the deprotonation of the functional groups and fCNT can be considered strongly anionic. According Clogston and Patri⁴⁵, nanoparticles with values greater than ± 30 mV are considered strongly cationic or anionic, while values between ± 10 mV, are considered neutral. In TiO₂-CNT sample, the nanoparticles are attached to the functional groups as evidenced above, neutralizing

the charge of the nanotubes and giving the sample a slightly positive charge. According Patri, TiO₂-CNT can be considered as neutral.

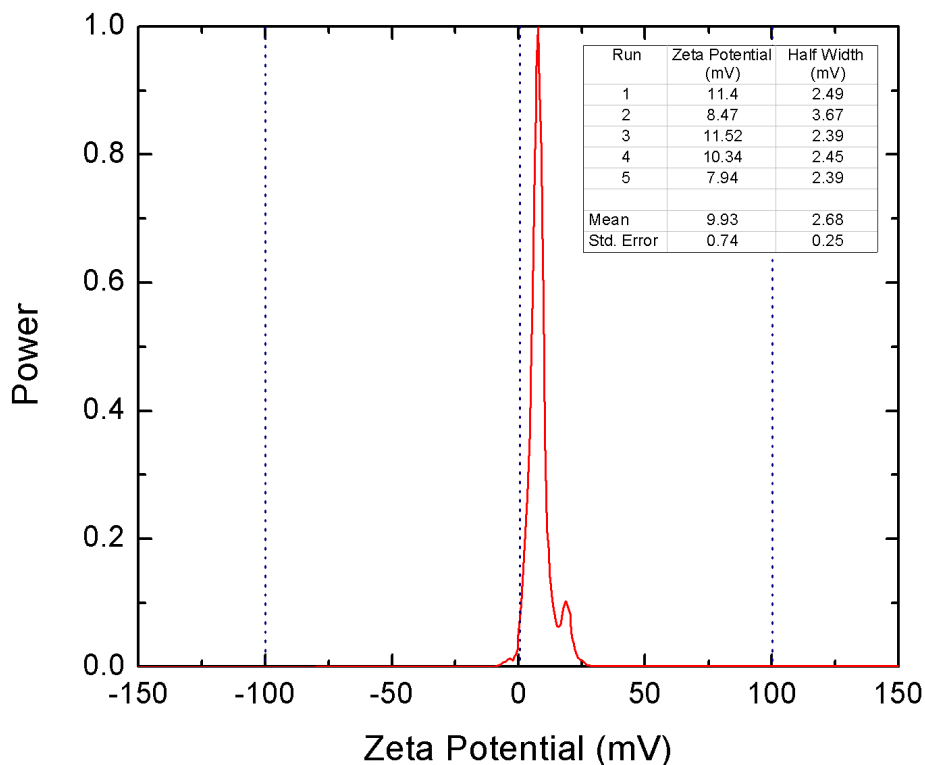


Figure 4.6: Zeta potential result for fCNTs showing a peak at 7.94 mV in the fifth run with a mean of -9.93 mV with a standard deviation of 0.74 mV.

Knowing the charge of the CNTs is essential to understand the interaction particle-solvent and predict a colloidal stability. The dispersion of the nanotubes plays a key role in the modification of the electrode. The selection of a solvent is quite a delicate issue depending the charge of the nanotubes. Specific differences in CNT dispersion arise from the geometry and polarity of the solvent molecules or the solubility of the polymer²² As we observe the charge of

the samples differs; the solvent in which the carbon nanotubes are suspended will be also different.

Dimethyl formamide (DMF) is a typical solvent of carbon nanotubes and it was selected to suspend fCNT. The suspension presented stability after a few minutes of sonication due the CNTs does not spontaneously disperse and requires an input of energy to achieve dispersion. The interaction of the solvent molecules with the nanotubes involves weak polar forces and van der Waals interactions. The DMF molecule is planar and provide a better engage through van der Waals interactions to the nanotube surface.

TiO₂-CNT sample present a different charge as fCNT and requires a different solvent. Vaisman²³ explained the use of surfactants to disperse nanotubes depending on their charge and type of surfactant. The selection of the surfactant depends on the charge the CNTs exhibit. The TiO₂-CNT sample was dispersed in a solution of sodium dodecyl sulfate (SDS). SDS is an anionic surfactant with a sulfate group at its head which gives it the amphiphilic properties. SDS debundles nanotubes through steric and electrostatic interactions. The anionic head of the surfactant molecule tends to attach to the nanotube walls and to be adsorbed over forming micelles and providing a colloidal stabilization.

4.3 Direct electrochemistry of modified and non-modified electrodes

The response evaluation of the electrodes in 0.1 M phosphate buffer solution at pH7 is presented in Figure 4.7, showing the voltammograms of the bare glassy carbon electrode, fCNT and TiO₂-CNT modified electrodes. This figure provides us the electroactive region of the electrodes, better called "window potential", and refers to the potential region where no redox events are present. The voltammogram of the bare (a) GCE does not exhibit any oxidation/reduction reaction. Very low non-faradaic current is shown in this region, exhibiting the current response almost flat.

The addition of the (b) fCNT shows a strong increment on the non-faradic current respect to the bare electrode. The non-faradaic current does not involve any electron transfer, it only causes the accumulation of electric charges as potential is applied⁶⁴. This result shows that functionalized CNTs exhibits a highly capacitive ability. The deposition of a wide enough layer

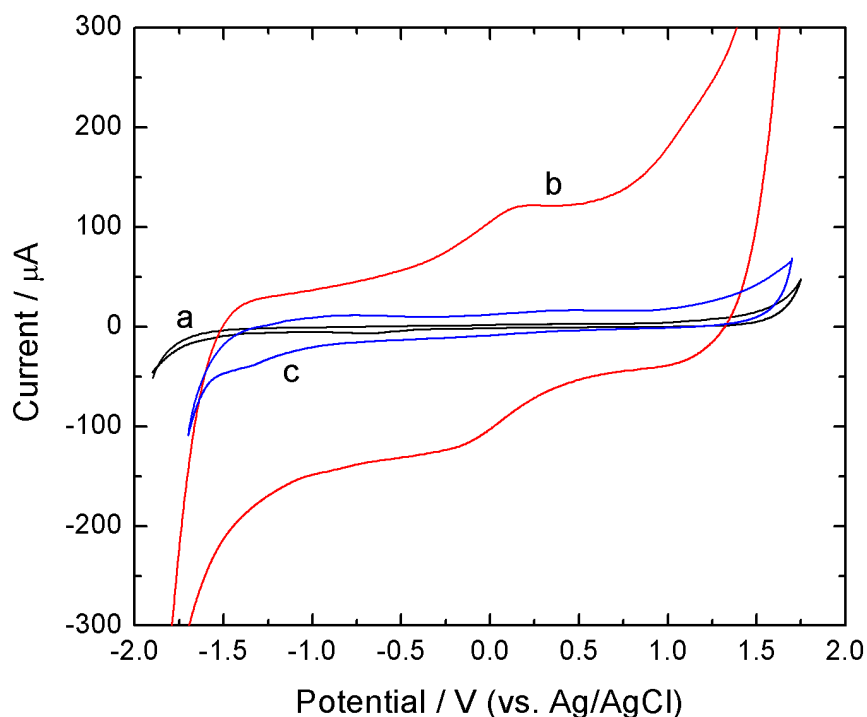


Figure 4.7: Electroactive region of (a) glassy carbon electrode, (b) fCNTs and (c) TiO₂-CNTs on PBS pH 7.

which implies the formation of an electric double layer. The presence of unexpected peaks along the window potential means there are at least one coupled reaction associated to the oxidation and reduction of the -OH and -COOH functional, leading to the formations of quinones around the surface of the nanotubes.

When (c) TiO₂-CNT is deposited over the electrode, the signal is similar respect to the bare GCE. There is not signals referred to the presence of electroactive species as expected while the non-faradaic current is a little higher respect to fCNTs. Modified nanotubes do not exhibit capacitive properties as sturdy as functionalized ones. The peaks around 0 and 0.3 V presented

in fCNTs are now disappeared, possible due to formation of the TiO₂ nanostructures over the functional groups, not allowing any redox process and leading the disappearance of the peaks. This result complements the interpretation for the physical characterization of the growth of the nanostructures around the -OH and -COOH group.

4.4 Evaluation response of modified and non-modified electrode in a redox system

The behavior of the electrodes is analyzed via an electrochemically electron transfer process, potassium ferricyanide is used. K₃[Fe(CN)₆] is a well-known redox specie commonly used. Potassium ferricyanide is used due to the nearly ideal reaction of the one-electron reduction of ferricyanide to ferrocyanide. In the PB/TiO₂-CNT and PB/CNT modified electrodes, the Prussian Blue layer acts as the redox specie. In the Prussian Blue layer also occurs a one-electron reduction in the Fe⁺³/Fe⁺² system.

Figure 4.8 displays the redox signal of the modified electrodes using potassium ferricyanide in the case of bare GCE, CNT/GCE, TiO₂-CNT/GCE, and Prussian Blue layer in PB/CNT/GCE and PB/TiO₂-CNT/GCE; at a scan rate of 100 mV/s. The I_{pa}/I_{pc} ratio is 1.02 of bare GCE (Figure 4.8 a), an expected value for a reversible reaction of charge transfer⁴². This value specifies if the oxidized analyte is all back reduced. For the bare electrode, this behavior is almost ideal as expected. The potential separation of the anodic and cathodic peak, potential difference (ΔE), is about 0.16 V. In a reversible reaction, ΔE must be constant and independent of scan rate, with a value close to 0.059 V. In this way, the value shows the reaction over a quasi-reversible process. Carbon-based electrodes are reported to exhibit this behavior due to low charge transfer rates respect to noble metal electrodes⁶⁵. For CNT/GCE, the peak ratio is 0.58 which indicates the a non-complete reversibility on the electrode; while ΔE is 0.21 V showing a higher resistance the layers produce. The TiO₂-CNT/GC electrode displays the I_{pa}/I_{pc} ratio of 0.69, showing a higher reversibility respect to the functionalized nanotubes. The ΔE is 0.22 V, similar to the fCNTs.

For the electrodes modified with Prussian Blue, the peak ratio is 0.5 showing a lower reversibility and ΔE is 0.18 V. Finally, the PB/TiO₂-CNT/GCE has a peak ratio of 0.62 and a ΔE

4.4. EVALUATION RESPONSE OF MODIFIED AND NON-MODIFIED ELECTRODE IN A REDOX SYSTEM

42

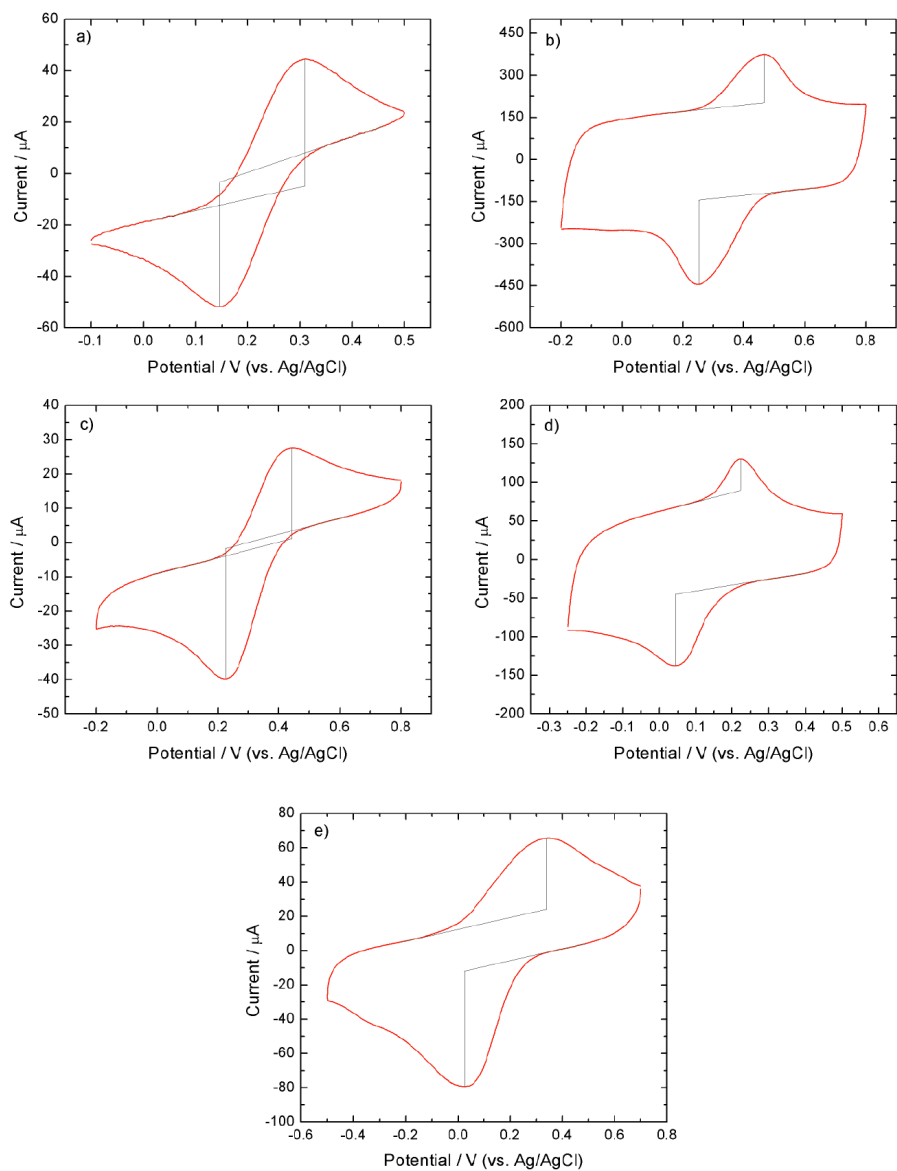


Figure 4.8: Cyclic voltammograms of the different GCE modifications at a scan rate of 100 mV/s. (a) Bare GCE, (b) CNT/GCE, (c) TiO₂-CNT/GCE, (d) PB/CNT/GCE and (e) PB/TiO₂-CNT/GCE.

value of 0.3 V. Comparing the results of the electrodes with and without the Prussian Blue layer, TiO₂-CNT exhibit a higher reversibility on the anodic and cathodic processes.

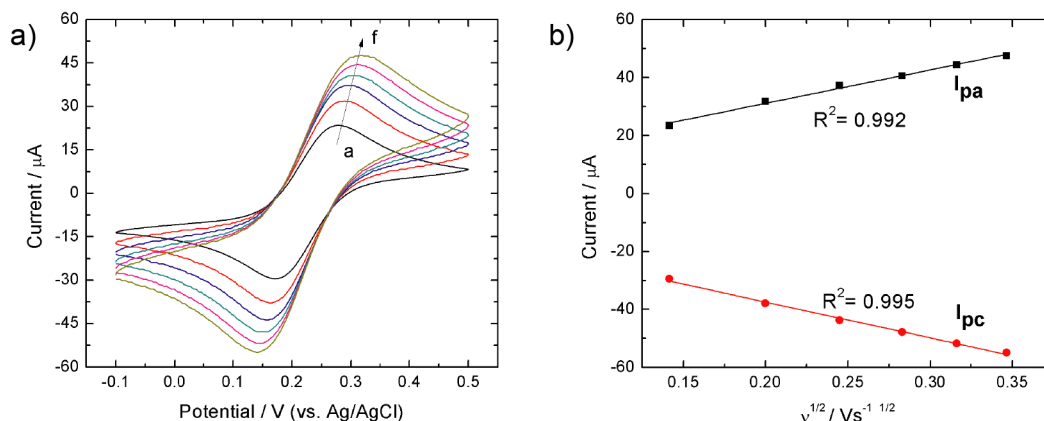


Figure 4.9: (a) Set of cyclic voltammeteries of the bare glassy carbon electrode at different scan rates (20-a, 40-b, 60-c ,80-d, 100-e, 120-f mV/s). (b) Linear regression of anodic (black line) and cathodic (red line) peak currents with correlation coefficients of 0.992 and 0.995, respectively

Figure 4.9a displays a set of cyclic voltammetry curves performed at different scan rates. An increment of the peak current is observed as scan rate varies. This current variation is proportional to each scan rate, while the potential peaks are practically no displaced. Considering these processes as reversible process, an electron transfer process of redox species, the Randles-Sevcik equation (Eq. 2.4) describes how the peak current changes linearly with the square root of the scan rate ' ν '. From this data, Figure 4.9a is created. The figure exhibits how the anodic and cathodic peak currents, and the square root of ν follow a linear behavior with a correlation coefficient of $R^2 = 0.992$ and 0.995 for the anodic and cathodic curve, respectively. This behavior is well explained in Randles-Sevcik equation indicating that the processes follow the diffusion of an electroactive specie. The intercept value of the line is 1.19×10^{-6} , a non-null value, which implies a small process of adsorption of ferricyanide over the electrode surface.

In the Figure 4.10, the same analysis is performed over the electrode with the functionalized

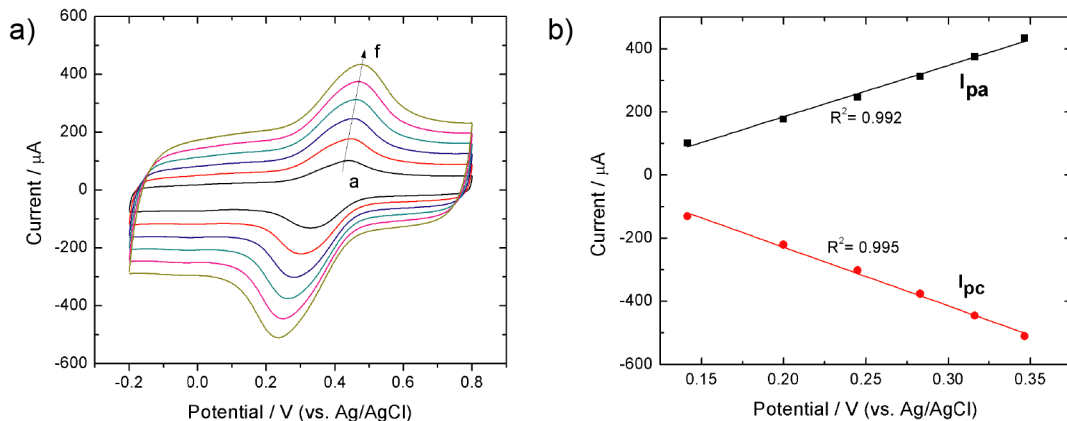


Figure 4.10: (a) Set of cyclic voltammograms of fCNT at different scan rates (20-a, 40-b, 60-c, 80-d, 100-e, 120-f mV/s). (b) Linear regression of anodic (black line) and cathodic (red line) peak currents with correlation coefficients of 0.992 and 0.995, respectively

CNTs. The behavior is similar with the currents increasing proportional to the scan rate and the potential peaks does maintain its potential. The correlation coefficients are 0.992 and 0.995 for the oxidation and reduction peaks, respectively. A non-null intersection, in this case a value of 1.4×10^{-4} , indicates a higher process of absorption of the iron complex in the CNT film. Potassium ferricyanide could even intercalate between the interlaminal spaces during voltammograms leading to a higher absorption into the nanotubes film⁶⁶.

The electrode modified with TiO_2 -CNTs displays the same behavior using potassium ferrocyanide as above Figure 4.11, with a correlation coefficients of 0.999 for anodic and cathodic processes. The interception value is $2.91 \cdot 10^{-6}$, which means a lower process of adsorption over the electrode surface.

The transfer process in the electrodes with Prussian Blue layer is directed by the one-electron reduction of the Prussian Blue layer to Prussian White; the reduction of the iron complex from Fe^{+3} to Fe^{+2} . The behavior is like the one with potassium ferrocyanide. The PB/CNT/GCE set of cyclic voltammograms has the current variation proportional to the scan rate. They are shown in

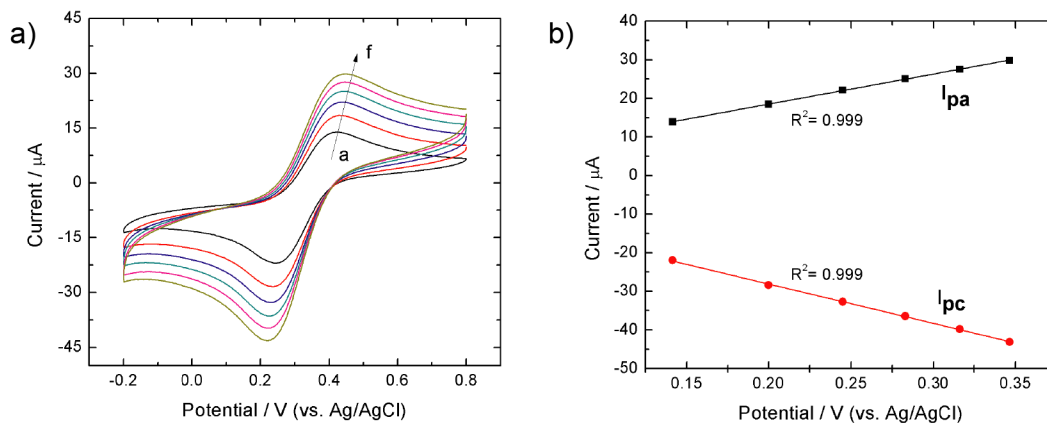


Figure 4.11: (a) Set of cyclic voltammograms of TiO₂-CNT at different scan rates (20-a, 40-b, 60-c, 80-d, 100-e, 120-f mV/s). (b) Linear regression of anodic (black line) and cathodic (red line) peak currents with correlation coefficients of 0.999 and 0.998, respectively.

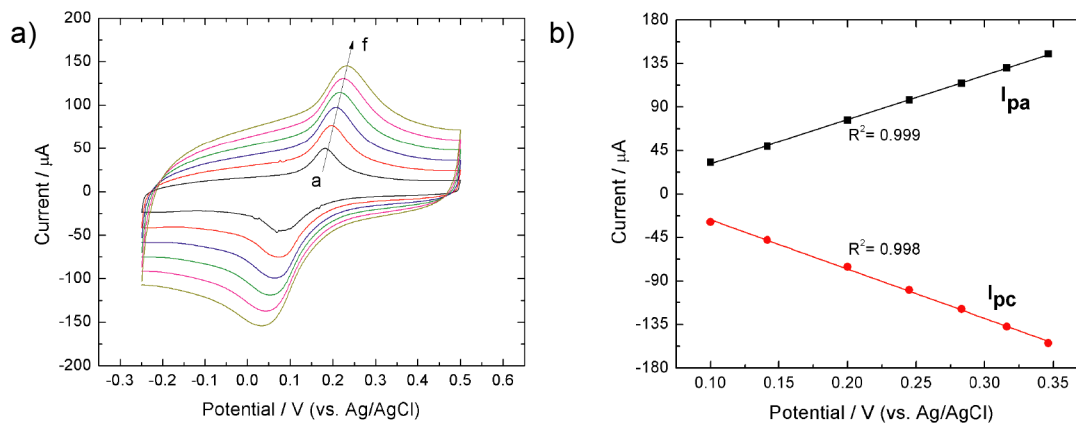


Figure 4.12: (a) Set of cyclic voltammograms of PB-CNT at different scan rates (20-a, 40-b, 60-c, 80-d, 100-e, 120-f mV/s). (b) Linear regression of anodic (black line) and cathodic (red line) peak currents with correlation coefficients of 0.999 and 0.998, respectively.

Figure 4.12. The correlation coefficients in the linear regression of the current peaks are 0.999 for the anodic process and 0.998 for the cathodic process.

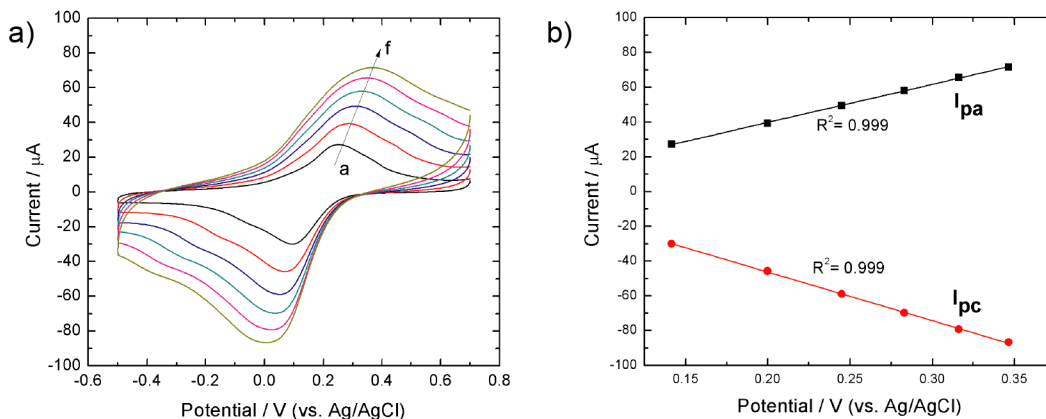


Figure 4.13: (a) Set of cyclic voltammograms of PB-TiO₂-CNT at different scan rates (20-a, 40-b, 60-c, 80-d, 100-e, 120-f mV/s). (b) Linear regression of anodic (black line) and cathodic (red line) peak currents with correlation coefficients of 0.999 and 0.999, respectively.

Figure 4.13 shows the change of current as the variation of scan rate in the PB/TiO₂-CNT/GC electrode. The current exhibits an excellent proportionality demonstrated in R² is 0.999 for anodic and cathodic behavior. Some shoulders appeared, possible due to the adsorption of Prussian Blue into deeper layers into the nanotubes, and non-uniform reduction and oxidation occur.

4.5 Electrochemistry of PB/CNT/GCE and PB/fCNT/GCE in presence of hydrogen peroxide via cyclic voltammetry

The catalytic activity of the Prussian blue in the detection of H₂O₂ is analyzed via cyclic voltammetry at different concentrations. This analysis is performed to see the contribution of TiO₂-CNT and fCNTs in the process of H₂O₂ detection. The detection is done analyzing the increment in the reduction current as the H₂O₂ concentration increases.

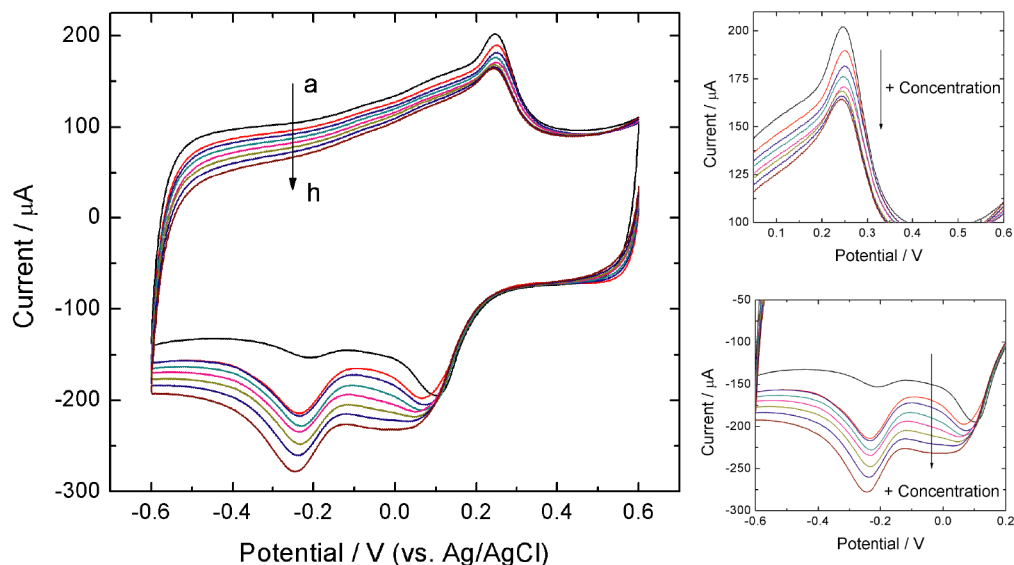


Figure 4.14: Set of cyclic voltammograms of PB-fCNT at different H_2O_2 concentrations (0.5 mM-a, 1.0 mM-b, 1.5 mM-c, 2.0 mM-d, 2.5 mM-e, 3.0 mM-f, 3.5 mM-g, and 4.0 mM-h). Reduction of anodic peak of Prussian Blue as H_2O_2 concentration increases (right, up). Increment of cathodic peak of Prussian Blue as H_2O_2 concentration increases (right, down).

Figure 4.14 exhibits the electrocatalytic behavior of the fCNTs and Prussian Blue. The peaks located at 0.2 and 0.1 V are attributed to the oxidation and reduction of Prussian Blue as shown before. The peak at 0.25 V coincides to the presence and reduction of H_2O_2 . It is clear to observe the proportional increment of the reduction current, while the PB oxidation peak decreases at each cycle and the PB reduction peak increases with the presence of H_2O_2 .

The reduction reaction of H_2O_2 induced by Prussian Blue has been found to be given by Equations 4.1, 4.2 and 4.3 and according Karyakin³⁹, the stability of Prussian Blue layer as hydrogen peroxide transducer is a crucial point due its thermodynamically instability³⁸. The presence of hydroxyl ions as products of the hydrogen peroxide reduction are able to solubilize

the Prussian Blue layer, producing an irreversible reaction. This is evidently in the decrement of the oxidation current of the inorganic polycrystal; PB had been consumed each cycle of detection.

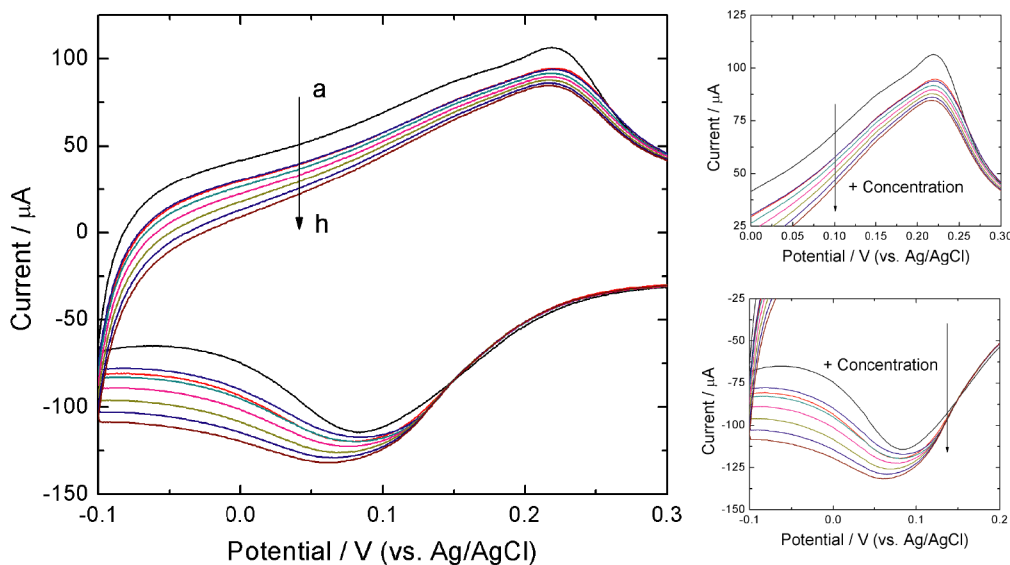


Figure 4.15: Set of cyclic voltammograms of PB-fCNT at different H_2O_2 concentrations (0.5 mM-a, 1.0 mM-b, 1.5 mM-c, 2.0 mM-d, 2.5 mM-e, 3.0 mM-f, 3.5 mM-g, and 4.0 mM-h) at a reduced potential range. Reduction of anodic peak of Prussian Blue as H_2O_2 concentration increases (right, up). Increment of cathodic peak of Prussian Blue as H_2O_2 concentration increases (right, down).

The detection was also performed with a short potential range to see only the behavior of the Prussian Blue peaks. Figure 4.15 exhibits peak responses, proportional with the variation of H_2O_2 . It demonstrates the catalytic activity of Prussian Blue over hydrogen peroxide and an outstanding proportionality. It is clear that the cathodic peak decreases and the anodic peak increases as expected. The detection was done from 0.5 mM to 4.0 mM H_2O_2 .

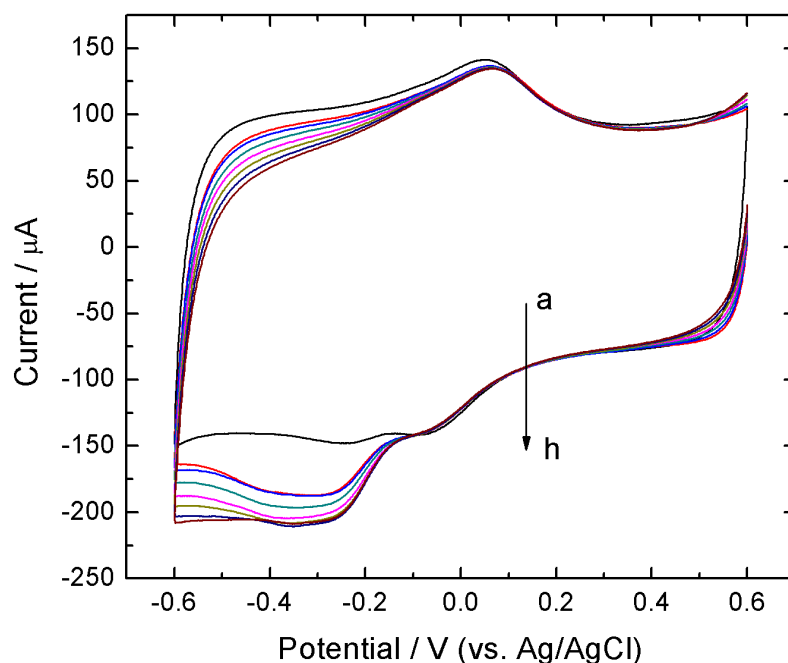


Figure 4.16: Set of cyclic voltammograms of fCNT at different H_2O_2 concentrations (0.5 mM-a, 1.0 mM-b, 1.5 mM-c, 2.0 mM-d, 2.5 mM-e, 3.0 mM-f, 3.5 mM-g, and 4.0 mM-h).

Figure 4.16 displays the detection of H_2O_2 in absence of the Prussian Blue layer under the same conditions. The peaks observed at 0.1 and -0.1 V are characteristic of the fCNTs and previously analyzed. Even with the absence of PB, the nanotubes partially allow the reduction of hydrogen peroxide. The response current does not present as good proportionality as previous experiments, but it demonstrates fCNTs actually contributes to the reduction of H_2O_2 . It validates

the fCNTs to be further used with peroxidases into enzyme-based biosensors.

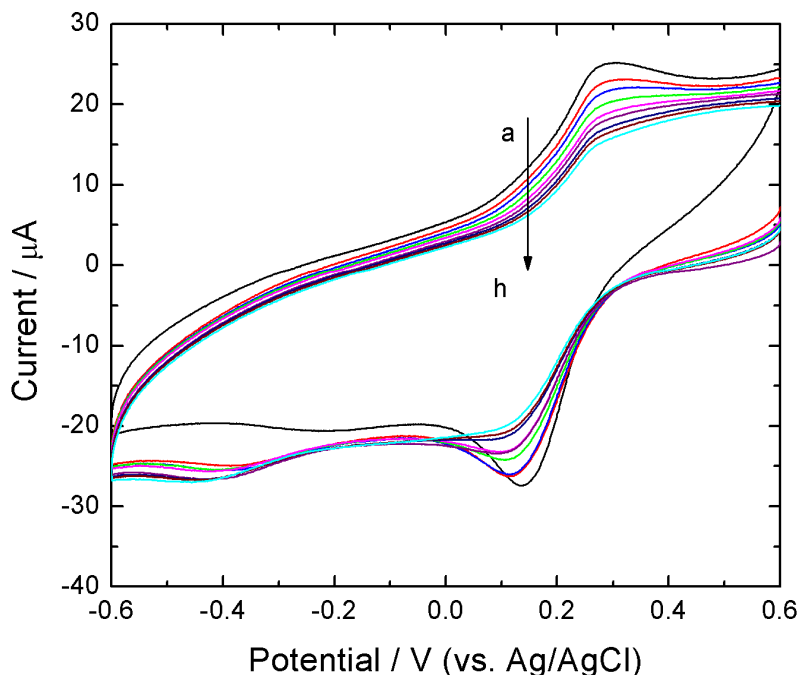


Figure 4.17: Set of cyclic voltammeteries of PB-fCNT at different H_2O_2 concentrations (0.5 mM-a, 1.0 mM-b, 1.5 mM-c, 2.0 mM-d, 2.5 mM-e, 3.0 mM-f, 3.5 mM-g, and 4.0 mM-h).

The detection was carried out with PB/TiO₂-CNT/GCE. Figure 4.17 exhibits the catalytic behavior of Prussian Blue based with TiO₂-CNTs. With the increase in concentration of hydrogen peroxide, the response of the electrode is not as expected. The reduction current is not proportional to the concentration, even when H_2O_2 is partially detected around 0.4 V. Comparing the TiO₂-CNT system along the fCNT one, it demonstrates that the presence of titanium dioxide does not provide an optimum interface for H_2O_2 detection. The oxidation peak of PB is the one that shows proportionality in the current response. The reduction peak does not show decreasing in current belonging to the reduction process of H_2O_2 ; it evidences the presence of hydrogen peroxide but not showing a high quality detection.

4.6 Evaluation response of PB/TiO₂-CNT/GCE and PB/fCNT/GCE in presence of hydrogen peroxide via amperometric i-t curve

The electrocatalysis of H₂O₂ based on Prussian Blue is followed by the Equation 4.3, reducing H₂O₂. The Prussian Blue reduces H₂O₂ approximately at 0.1 V. The applied potential to perform the amperometric curves was selected below the reduction potential, at 0 V, where the current is dictated via diffusion from the bulk solution to the electrode, after the analyte is steadily depleted over the electrode surface.

The steady-state current response of H₂O₂ in the PB/fCNT/GCE is shown in Figure 4.18a. The current response decreases with increasing the H₂O₂ concentration with successive injections of 100 μ L of 0.1 M in 20 mL of PBS. The trace demonstrates high sensitivity and response of the sensor. The electrode reached 95 % of the maximum steady-state current in less than 10 seconds which indicates a fast response. A linear range from 500 μ M to 6.54 mM is obtained, showing a high linearity of the response. Figure 4.18b displays the calibration curve of the sensor. The linear regression equation can be expressed as Equation 4.4 with a correlation coefficient of 0.992.

$$I(\mu\text{A}) = -16.30(\text{mM}) - 8.535 \cdot 10^{-6} \quad (4.4)$$

The sensitivity given by the slope of the linear regression corresponds to 16.30 μ A/mM, the limit of detection calculated from the quotient of 3 times the standard deviation (SD) of blank and the sensitivity is 0.015 mM and the limit of quantification, calculated from the quotient of 10 times the SD with the sensitivity is 0.051 mM. Nevertheless, carbon nanotubes show linear and fast response being candidates to prove an enzymatic electrode.

Figure 4.19a shows the amperometric response of the PB/TiO₂-CNT/GCE for the successive additions of H₂O₂ under the same parameters as fCNT to compare the quality response of both systems. The electrode has a fast response and high sensitivity. Also, this system exhibit two linear responses displayed in the calibration curve (Figure 4.19b). This behavior can be attributed

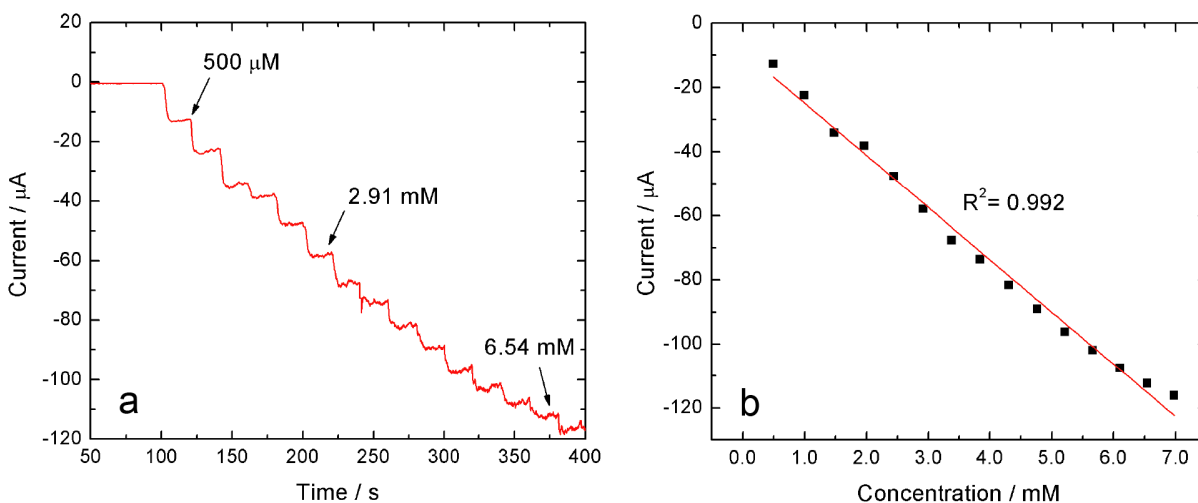


Figure 4.18: (a) Dynamic response of the H₂O₂ on fCNT/GC electrode to the successive addition of 100 μL of 0.1 M H₂O₂ in the PBS solution at 0.5 V. (b) Calibration curve of the amperometric response between the current and H₂O₂ concentration.

to the saturation of the electrode with H₂O₂, leading to the corresponding decrement in the sensitivity.

The linear regression to the dynamic response of the electrode is shown in Figure 4.19b. Two linear ranges are observed from 500 μM to 3.84 mM, and from 4.76 mM to 6.54 mM. From these ranges, each one is fitted given the Equations 4.5 and 4.6 with correlation coefficients of 0.980 and 0.996, respectively. The sensitivity for the first range, corresponding to the slope of the first regression, is 26.51 $\mu\text{A}/\text{mM}$, while the sensitivity for the second linear range decreases to 10.17 $\mu\text{A}/\text{mM}$, higher values than the ones reported by Yu in H₂O₂ detection over only a titania matrix⁶⁷. This result leads to a limit of detection of 0.092 mM and a limit of quantification of 0.31 mM, showing that fCNTs displays higher sensitivity and linear response compared to TiO₂-CNTs in H₂O₂ detection.

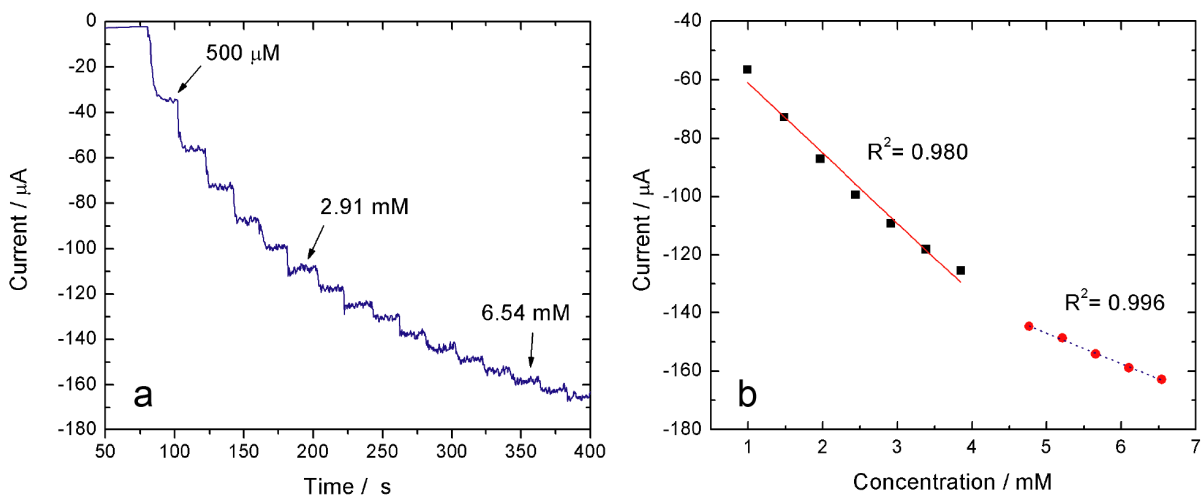


Figure 4.19: (a) Dynamic response of the H₂O₂ on TiO₂CNT/GC electrode to the successive addition of 100 μL of 0.1 M H₂O₂ in the PBS solution at 0.5 V. (b) Calibration curve of the amperometric response between the current and H₂O₂ concentration.

$$I(\mu\text{A}) = -24.01(\text{mM}) - 37.16 \cdot 10^{-6} \quad (4.5)$$

$$I(\mu\text{A}) = -10.42(\text{mM}) - 94.82 \cdot 10^{-6}, \quad (4.6)$$

The overall experiments proves that the presence of titanium dioxide over the walls of the carbon nanotubes does not provide an enhanced interface on detection of H₂O₂ compared to functionalized carbon nanotubes. The addition of TiO₂ was considered due to its well-known properties of biocompatibility, but the presence of hydroxyl and carboxylic groups in fCNTs could provide a better bonding formation with the inorganic polycrystal. The TiO₂ nanostructures seem that occur over the -OH and -COOH groups decreasing the adequate bonding with H₂O₂ molecules, allowing the saturation of the electrode at higher H₂O₂ concentrations.

In both cases, carbon nanotubes contribute to an interface for an effective detection of H₂O₂ along the catalytic activity of Prussian Blue, but leading the limit of detection of TiO₂-CNT electrode be five times higher than fCNT electrode. In future research, the immobilization of

4.6. *EVALUATION RESPONSE OF PB/TIO₂-CNT/GCE AND PB/FCNT/GCE IN PRESENCE OF HYDROGEN PEROXIDE VIA AMPEROMETRIC I-T CURVE*

biomolecules as enzymes (horseradish peroxidase or glucose oxidase) could be successfully achieved with the presence of titanium dioxide nanostructures maintaining a biocompatible route of interfacing.

Chapter 5

Conclusions

The main objective of this research was to design an electrochemical biosensor based on multi-walled carbon nanotubes modified with titania nanostructures (TiO₂-MWCNTs) for hydrogen peroxide (H₂O₂) detection. The study included the comparison of TiO₂-MWCNTs performance over functionalized MWCNTs (fMWCNTs) in sensitivity and limit of detection in H₂O₂ reduction.

From physical characterization, the presence of TiO₂ nanostructures was confirmed over the carbon nanotubes walls. Via XRD, the TiO₂ crystalline phase was corroborated to be anatase with structures around 6 nm, and carbon nanotubes around 4-10 layers with a mean diameter of 5 ± 2 nm. FTIR spectra also confirmed the presence of TiO₂ establishing the band of Ti-O-Ti vibrations in the fingerprint region.

Zeta potential characterization demonstrated the different surface charges that fMWCNTs (-52 mV) and TiO₂-MWCNTs (10 mV) exhibit. These charges allowed the dispersion of the samples in different media: dimethyl formamide (DMF) for fMWCNTs, and sodium dodecylsulfate (SDS) for TiO₂-MWCNTs. The variation on the dispersion led to an appropriate electrostatic stabilization of the CNTs over the glassy carbon electrode in the modification process. The presence of PDDA also contributed to this stabilization.

The bare and modified electrodes were electrochemically characterized in phosphate buffer solution providing information about the electroactive region of electrodes (from 1.25 to -1.25

V). The non-faradaic current remains similar between the bare and TiO₂-MWCNT modified electrode, while fMWCNT electrode exhibited a strong increment in the non-faradic response, showing a high capacitive ability.

The detection of hydrogen peroxide was evaluated via cyclic voltammetry (CV) and amperometric i-t curve to analyze the reduction of H₂O₂ through the electrocatalytic activity of Prussian Blue. The CV curves showed an irreversible reaction of Prussian Blue reducing H₂O₂ due to the formation of OH⁻. The presence of OH⁻ ions solubilizes the Prussian Blue layer confirming the irreversible reaction. It was demonstrated the increment on current response as H₂O₂ concentration increases, showing a higher proportionality current-concentration in fMWCNTs respect to TiO₂-MWCNTs.

Amperometric curve showed the typical current response after successive injections of H₂O₂. In both cases, the electrodes reached a 95% of the maximum steady-state current in less than 10 seconds, showing a fast response and high sensitivity. Linear calibration of the amperometric curves exhibited sensitivity, limit of detection and limit of quantification for fMWCNTs as 16.30 μA/mM, 0.015 mM and 0.051 mM, respectively. For TiO₂-MWCNTs, the sensitivity, limit of detection and limit of quantification were 26.51 μA/mM, 0.092 mM and 0.31 mM, respectively. It demonstrates the higher sensitivity of the fMWCNTs respect to TiO₂-MWCNTs.

Bibliography

- [1] Choudhary, V.; Gupta, A. *Carbon nanotubes-polymer nanocomposites*; IntechOpen, 2011.
- [2] Bhat, S.; Kumar, A. Biomaterials and bioengineering tomorrow's healthcare. *Biomatter* **2013**, *3*, e24717.
- [3] Wang, J. Carbon-nanotube based electrochemical biosensors: A review. *Electroanalysis: An International Journal Devoted to Fundamental and Practical Aspects of Electroanalysis* **2005**, *17*, 7–14.
- [4] Eatemadi, A.; Daraee, H.; Karimkhanloo, H.; Kouhi, M.; Zarghami, N.; Akbarzadeh, A.; Abasi, M.; Hanifehpour, Y.; Joo, S. W. Carbon nanotubes: properties, synthesis, purification, and medical applications. *Nanoscale research letters* **2014**, *9*, 393.
- [5] Stobbe, S.; Lindelof, P.; Nygård, J. Integration of carbon nanotubes with semiconductor technology: fabrication of hybrid devices by III–V molecular beam epitaxy. *Semiconductor science and technology* **2006**, *21*, S10.
- [6] Charlier, J.-C. Defects in carbon nanotubes. *Accounts of chemical research* **2002**, *35*, 1063–1069.
- [7] Gong, K.; Yan, Y.; Zhang, M.; SU, L.; XIONG, S.; MAO, L. Electrochemistry and electroanalytical applications of carbon nanotubes: a review. *Analytical sciences* **2005**, *21*, 1383–1393.
- [8] Thévenot, D. R.; Toth, K.; Durst, R. A.; Wilson, G. S. Electrochemical biosensors: recommended definitions and classification. *Analytical Letters* **2001**, *34*, 635–659.

- [9] Solanki, P. R.; Kaushik, A.; Agrawal, V. V.; Malhotra, B. D. Nanostructured metal oxide-based biosensors. *NPG Asia Materials* **2011**, *3*, 17.
- [10] Han, F.; Kambala, V. S. R.; Srinivasan, M.; Rajarathnam, D.; Naidu, R. Tailored titanium dioxide photocatalysts for the degradation of organic dyes in wastewater treatment: a review. *Applied Catalysis A: General* **2009**, *359*, 25–40.
- [11] Bai, J.; Zhou, B. Titanium dioxide nanomaterials for sensor applications. *Chemical reviews* **2014**, *114*, 10131–10176.
- [12] Rhee, S. G.; Chang, T.-S.; Jeong, W.; Kang, D. Methods for detection and measurement of hydrogen peroxide inside and outside of cells. *Molecules and cells* **2010**, *29*, 539–549.
- [13] Grisham, M. B. Methods to detect hydrogen peroxide in living cells: Possibilities and pitfalls. *Comparative Biochemistry and Physiology Part A: Molecular & Integrative Physiology* **2013**, *165*, 429–438.
- [14] Karyakin, A. A.; Gitelmacher, O. V.; Karyakina, E. E. A high-sensitive glucose amperometric biosensor based on Prussian Blue modified electrodes. *Analytical Letters* **1994**, *27*, 2861–2869.
- [15] Sajjadi, S.; Keihan, A. H.; Norouzi, P.; Habibi, M. M.; Eskandari, K.; Shirazi, N. H. Fabrication of an Amperometric Glucose Biosensor Based on a Prussian Blue/Carbon Nanotube/Ionic Liquid Modified Glassy Carbon Electrode. *Journal of Applied Biotechnology Reports* **2017**, *4*, 603–608.
- [16] Evans, S. A.; Elliott, J. M.; Andrews, L. M.; Bartlett, P. N.; Doyle, P. J.; Denuault, G. Detection of hydrogen peroxide at mesoporous platinum microelectrodes. *Analytical Chemistry* **2002**, *74*, 1322–1326.
- [17] Jeevanandam, J.; Barhoum, A.; Chan, Y. S.; Dufresne, A.; Danquah, M. K. Review on nanoparticles and nanostructured materials: history, sources, toxicity and regulations. *Beilstein journal of nanotechnology* **2018**, *9*, 1050–1074.
- [18] Roduner, E. Size matters: why nanomaterials are different. *Chemical Society Reviews* **2006**, *35*, 583–592.

- [19] Ma, P.-C.; Siddiqui, N. A.; Marom, G.; Kim, J.-K. Dispersion and functionalization of carbon nanotubes for polymer-based nanocomposites: a review. *Composites Part A: Applied Science and Manufacturing* **2010**, *41*, 1345–1367.
- [20] Xie, X.-L.; Mai, Y.-W.; Zhou, X.-P. Dispersion and alignment of carbon nanotubes in polymer matrix: a review. *Materials science and engineering: R: Reports* **2005**, *49*, 89–112.
- [21] Dresselhaus, G.; Riichiro, S. *Physical properties of carbon nanotubes*; World scientific, 1998.
- [22] Pramanik, C.; Gissinger, J. R.; Kumar, S.; Heinz, H. Carbon nanotube dispersion in solvents and polymer solutions: mechanisms, assembly, and preferences. *ACS nano* **2017**, *11*, 12805–12816.
- [23] Vaisman, L.; Wagner, H. D.; Marom, G. The role of surfactants in dispersion of carbon nanotubes. *Advances in colloid and interface science* **2006**, *128*, 37–46.
- [24] Tang, H.; Prasad, K.; Sanjines, R.; Schmid, P.; Levy, F. Electrical and optical properties of TiO₂ anatase thin films. *Journal of applied physics* **1994**, *75*, 2042–2047.
- [25] Chen, X.; Mao, S. S. Titanium dioxide nanomaterials: synthesis, properties, modifications, and applications. *Chemical reviews* **2007**, *107*, 2891–2959.
- [26] others., *et al.* A review on the visible light active titanium dioxide photocatalysts for environmental applications. *Applied Catalysis B: Environmental* **2012**, *125*, 331–349.
- [27] Haider, A. J.; Jameel, Z. N.; Al-Hussaini, I. H. Review on: Titanium Dioxide Applications. *Energy Procedia* **2019**, *157*, 17–29.
- [28] Akpan, U.; Hameed, B. The advancements in sol–gel method of doped-TiO₂ photocatalysts. *Applied Catalysis A: General* **2010**, *375*, 1–11.
- [29] Thevenot, D. R.; Toth, K.; Durst, R. A.; Wilson, G. S. Electrochemical biosensors: recommended definitions and classification. *Pure and applied chemistry* **1999**, *71*, 2333–2348.

- [30] Mehrotra, P. Biosensors and their applications—A review. *Journal of oral biology and craniofacial research* **2016**, *6*, 153–159.
- [31] Li, Y.; Schluesener, H. J.; Xu, S. Gold nanoparticle-based biosensors. *Gold Bulletin* **2010**, *43*, 29–41.
- [32] Biju, V. Chemical modifications and bioconjugate reactions of nanomaterials for sensing, imaging, drug delivery and therapy. *Chemical Society Reviews* **2014**, *43*, 744–764.
- [33] Zhang, C.-Y.; Yeh, H.-C.; Kuroki, M. T.; Wang, T.-H. Single-quantum-dot-based DNA nanosensor. *Nature materials* **2005**, *4*, 826.
- [34] Putzbach, W.; Ronkainen, N. Immobilization techniques in the fabrication of nanomaterial-based electrochemical biosensors: A review. *Sensors* **2013**, *13*, 4811–4840.
- [35] Johansson, I.; Somasundaran, P. *Handbook for Cleaning/decontamination of Surfaces*; Elsevier, 2007.
- [36] Itaya, K.; Shoji, N.; Uchida, I. Catalysis of the reduction of molecular oxygen to water at Prussian blue modified electrodes. *Journal of the American Chemical Society* **1984**, *106*, 3423–3429.
- [37] Neff, V. D. Electrochemical oxidation and reduction of thin films of Prussian Blue. *Journal of the Electrochemical Society* **1978**, *125*, 886–887.
- [38] Karyakin, A. A. Prussian blue and its analogues: electrochemistry and analytical applications. *Electroanalysis: An International Journal Devoted to Fundamental and Practical Aspects of Electroanalysis* **2001**, *13*, 813–819.
- [39] Karyakin, A. A.; Karyakina, E. E.; Gorton, L. On the mechanism of H₂O₂ reduction at Prussian Blue modified electrodes. *Electrochemistry Communications* **1999**, *1*, 78–82.
- [40] Settle, F. *Handbook of instrumental techniques for analytical chemistry*. 2002.
- [41] Kissinger, P. T.; Heineman, W. R. Cyclic voltammetry. *Journal of Chemical Education* **1983**, *60*, 702.

- [42] Elgrishi, N.; Rountree, K. J.; McCarthy, B. D.; Rountree, E. S.; Eisenhart, T. T.; Dempsey, J. L. A practical beginner's guide to cyclic voltammetry. *Journal of chemical education* **2017**, *95*, 197–206.
- [43] Bard, A. J.; Faulkner, L. R.; Leddy, J.; Zoski, C. G. *Electrochemical methods: fundamentals and applications*; Wiley New York, 1980; Vol. 2.
- [44] Kirby, B. J.; Hasselbrink Jr, E. F. Zeta potential of microfluidic substrates: 1. Theory, experimental techniques, and effects on separations. *Electrophoresis* **2004**, *25*, 187–202.
- [45] Clogston, J. D.; Patri, A. K. *Characterization of nanoparticles intended for drug delivery*; Springer, 2011; pp 63–70.
- [46] Hunter, R. J. *Zeta potential in colloid science: principles and applications*; Academic press, 2013; Vol. 2.
- [47] Nikhil Bhalla, N. F. P. E., Pawan Jolly Introduction to biosensors. *Essays in Biochemistry* **2016**, *60*, 1–8.
- [48] Liu, Y.; Wang, M.; Zhao, F.; Xu, Z.; Dong, S. The direct electron transfer of glucose oxidase and glucose biosensor based on carbon nanotubes/chitosan matrix. *Biosensors and Bioelectronics* **2005**, *21*, 984–988.
- [49] Qian, L.; Yang, X. Composite film of carbon nanotubes and chitosan for preparation of amperometric hydrogen peroxide biosensor. *Talanta* **2006**, *68*, 721–727.
- [50] Besteman, K.; Lee, J.-O.; Wiertz, F. G.; Heering, H. A.; Dekker, C. Enzyme-coated carbon nanotubes as single-molecule biosensors. *Nano letters* **2003**, *3*, 727–730.
- [51] Fotouhi, L.; Dorraji, P. S.; Keshmiri, Y. S. S.; Hamtak, M. Electrochemical Sensor Based on Nanocomposite of Multi-Walled Carbon Nanotubes/TiO₂ Nanoparticles in Chitosan Matrix for Simultaneous and Separate Determination of Dihydroxybenzene Isomers. *Journal of The Electrochemical Society* **2018**, *165*, B202–B211.
- [52] Zhang, M.; Yuan, R.; Chai, Y.; Li, W.; Zhong, H.; Wang, C. Glucose biosensor based on titanium dioxide-multiwall carbon nanotubes-chitosan composite and functionalized gold nanoparticles. *Bioprocess and biosystems engineering* **2011**, *34*, 1143–1150.

- [53] Kafi, A.; Wu, G.; Chen, A. A novel hydrogen peroxide biosensor based on the immobilization of horseradish peroxidase onto Au-modified titanium dioxide nanotube arrays. *Biosensors and Bioelectronics* **2008**, *24*, 566–571.
- [54] Shen, Q.; You, S.-K.; Park, S.-G.; Jiang, H.; Guo, D.; Chen, B.; Wang, X. Electrochemical biosensing for cancer cells based on TiO₂/CNT nanocomposites modified electrodes. *Electroanalysis: An International Journal Devoted to Fundamental and Practical Aspects of Electroanalysis* **2008**, *20*, 2526–2530.
- [55] Kiema, G. K.; Aktay, M.; McDermott, M. T. Preparation of reproducible glassy carbon electrodes by removal of polishing impurities. *Journal of Electroanalytical Chemistry* **2003**, *540*, 7–15.
- [56] Hobbs, J. M.; Patel, N. N.; Kim, D. W.; Rugutt, J. K.; Wanekaya, A. K. Glucose determination in beverages using carbon nanotube modified biosensor: an experiment for the undergraduate laboratory. *Journal of Chemical Education* **2013**, *90*, 1222–1226.
- [57] Kharissova, O. V.; Kharisov, B. I. Variations of interlayer spacing in carbon nanotubes. *Rsc Advances* **2014**, *4*, 30807–30815.
- [58] Sharon, M.; Modi, F.; Sharon, M. Titania based nanocomposites as a photocatalyst: A review. *AIMS Materials Science* **2016**, *3*, 1236–1254.
- [59] Patterson, A. The Scherrer formula for X-ray particle size determination. *Physical review* **1939**, *56*, 978.
- [60] Atieh, M. A.; Bakather, O. Y.; Al-Tawbini, B.; Bukhari, A. A.; Abuilaiwi, F. A.; Fet-touhi, M. B. Effect of carboxylic functional group functionalized on carbon nanotubes surface on the removal of lead from water. *Bioinorganic chemistry and applications* **2010**, *2010*.
- [61] do Amaral Montanheiro, T. L.; Cristóvan, F. H.; Machado, J. P. B.; Tada, D. B.; Durán, N.; Lemes, A. P. Effect of MWCNT functionalization on thermal and electrical properties of PHBV/MWCNT nanocomposites. *Journal of Materials Research* **2015**, *30*, 55–65.

- [62] Albano, C.; Sarmiento, Y.; González, G. Synthesis and Characterization of Nanostructures: MWCNTf/TiO₂ and MWCNTf/TiO₂/HAp. 2012.
- [63] Kaszuba, M.; Corbett, J.; Watson, F. M.; Jones, A. High-concentration zeta potential measurements using light-scattering techniques. *Philosophical Transactions of the Royal Society A: Mathematical, Physical and Engineering Sciences* **2010**, *368*, 4439–4451.
- [64] Biesheuvel, P.; Dykstra, J. The difference between Faradaic and Nonfaradaic processes in Electrochemistry. *arXiv preprint arXiv:1809.02930* **2018**,
- [65] Wightman, R. M.; Deakin, M. R.; Kovach, P. M.; Kuhr, W. G.; Stutts, K. J. Methods to improve electrochemical reversibility at carbon electrodes. *Journal of the Electrochemical Society* **1984**, *131*, 1578–1583.
- [66] Wang, J.; You, J.; Li, Z.; Yang, P.; Jing, X.; Cao, D.; Zhang, M. Electrochemical performance of Ni/Al hydrotalcite supported on porous nickel electrode in hexacyanoferrate (III) media. *Solid State Sciences* **2008**, *10*, 1093–1098.
- [67] Yu, J.; Ju, H. Preparation of porous titania Sol- Gel matrix for immobilization of horseradish peroxidase by a vapor deposition method. *Analytical chemistry* **2002**, *74*, 3579–3583.